NTNU

Norwegian University of
Science and Technology

Comprehensive comparison of analytical wind turbine wake models with wind tunnel measurements and wake model application on performance modelling of a downstream turbine

Marian Felix Polster

Master of Energy and Environmental Engineering
Submission date: July 2017
Supervisor: Lars Sætran, EPT

Norwegian University of Science and Technology
Department of Energy and Process Engineering

Acknowledgement

I would like to thank professor Lars Sætran for giving me the opportunity to write my thesis at the NTNU in Trondheim and for supervision of my work. Furthermore, I would like to thank Jan Bartl and Franz Mühle for always supporting me with technical and non-technical problems. Moreover, I would like to thank them for giving me the possibility to use their gathered wind tunnel measurements. All test case B and C measurements used in this work were originally conducted by the two of them. Finally, I would like to thank Luis Garcia with whom I conducted the test case A measurements together.

Abstract

Wake effects in wind farms can cause significant power losses. In order to reduce these losses layout and control optimization can be applied. For this purpose, simple and fast tools to predict the wake flow are needed. In the first part of this work, six analytical wind turbine wake models are compared to extensive small-scale turbine wind tunnel measurements. The measurements are conducted at several downstream distances, varying the ambient turbulence intensity and the upstream turbine blade pitch angle. Furhermore, an adjustment of a recently developed wake model is proposed. Subsequently, the adjusted model is found to perform best throughout all test cases. In the second part, this wake model is used to predict the performance of a downstream turbine. In order to consider the non-uniform inflow velocity a mean-blade-element-velocity method is developed. Additionally, this method is compared to a simple method, which averages the velocity over the entire rotor area. Moreover, a Blade Element Momentum method with guaranteed convergence [1] and blockage effect correction [2] are applied. Finally, the simulations are compared to comprehensive wind tunnel measurements. In total, this approach is found to predict the wake velocity as well as the combined power of two aligned turbines fairly well.

1 Introduction

Wind turbines are usually clustered as wind farms to share the infrastructure and thus reduce the cost of energy. This results in an aerodynamic interaction between the wind turbines. Inside a wind farm the upstream wind turbines convert the kinetic energy in the wind into mechanical energy. Due to conservation of energy a velocity deficit in the flow behind the upstream turbine, called wake, can be observed. The wake can be divided into near and far wake. The near wake is defined as the region just behind the rotor, where the rotor characteristics such as number of blades and blade aerodynamics influence the velocity deficit. Whereas the far wake is defined as the area, where the actual rotor shape is less important [3]. According to Sørensen et al. [4] the near wake length is the downstream distance, from where a fully developed Gaussian wake shape can be observed. Downstream turbines located in the wake experience this velocity deficit and consequently produce less energy compared to non-disturbed conditions. Therefore, average wind farm power losses due to wind turbine wakes are in the range of 10 - 20 % in large offshore wind farms [5]. For low turbine spacing as in case of Lillgrund offshore wind farm the power loss can amount up to 23 % [6]. Furthermore, several numerical and experimental studies revealed an increasing level of turbulence intensity within the wake [7]. High turbulence intensities can lead to decreased lifespan and increased maintenance cost [8]. Hence, due to velocity deficits and increased loads the wake effect has a strong influence on wind farm profitability.

In order to reduce these effects wind farm planers can optimise a wind farm layout during the planning period using commercial software like WindPRO [9]. Another method for wind farm operators is to optimise wind farm control. Whereas traditional control strategies aim to maximise a single turbine power output, optimised wind farm control intends to maximise the overall wind farm power output. This can be achieved by reducing the upstream turbines energy extraction through tip speed ratio or blade pitch variations away from the design point. Several studies found a gain in wind farm efficiency by applying wind farm control [10] [11] [12]. For both, wind farm layout and control optimisation, an accurate prediction of wind turbine wakes is crucial. Due to their simplicity and low computational time, analytical wake models are widely used for this purpose.

One of the pioneering analytical single wake models is the one proposed by N.O. Jensen [13] in 1983. The model is based on conservation of momentum and assumes a uniform velocity profile inside the wake. Furthermore, it includes a constant approximated thrust coefficient. Katic et al. [14] further developed this model in 1986 taking wind turbine characteristics such as a variable thrust coefficient into account. This model is widely known as the Jensen model or PARK model. Later, in 1988 G.C. Larsen [15] proposed a Gaussian-shape wake model, which is based on Prandtl's turbulent boundary layer equation. Larsen himself improved this model in 2009 [16] by applying empirically determined boundary conditions. In 2004, Ishihara et al. [17] developed a wake model, which for the first time takes the effect of turbulence intensity in the wake on the wake recovery into account. Subsequently, in 2006, Frandsen et al. [18] proposed another top-hat shape single wake model for modelling of wind farm efficiencies. A recently developed analytical wake model is the one proposed by Bastankah & Porté-Agel [19] in 2014. The model predicts a Gaussian wake shape and is derived by applying mass and momentum conservation. One of the newest analytical wake models is the one proposed by Gao et al. [20] in 2016. It is based on the Jensen model using a Gaussian wake shape. Furthermore, the model includes a new turbulence intensity model, which takes ambient and rotor added turbulence intensity into account.

Besides a precise wake prediction an accurate mod-

elling of wind turbine power and thrust is crucial. This can be done numerically either by Computational Fluid Dynamics (CFD) simulations combined with the actuator line model or solving the Blade-Element Momentum (BEM) equations. The BEM method is a widely used design and analysis method. Already in 1935, H. Glauert proposed a solution of the BEM theory, which discretises the blade into annular element and uses an iterative approached to calculate the axial and tangential forces independently for each blade element [21]. In recent years various improvements to the solution method were done to account for convergence problems [22] [23], which still faced few difficulties [1]. Recently, S. Ning proposed a solution method, which includes a robust and efficient root-finding algorithm with guaranteed convergence [1].

2 Methods

In this section, the methodology of this work is presented. At first, the wind tunnel experiments are described in detail. Subsequently, the applied blockage effect correction method is described and derived. Furthermore, the analytical wake models for predicting the wake flow are presented. Finally, the Blade Element Momentum method with guaranteed convergence including a solution for a non-uniform inflow is described.

2.1 Experimental description

All experiments are conducted in the closed-loop wind tunnel at Norwegian University of Science and Technology (NTNU) in Trondheim. The wind tunnel consists of a test section of 2.71 m width, 1.81 m height and 11.15 m length. In this work, the streamwise direction is defined as x, the horizontal spanwise direction as z and the vertical spanwise direction as y.

Measurements with three wind turbines are performed. An overview of the wind turbine characteristics is given in Table 1. Herein, turbine T1 and T2 have exactly the same blade geometry. The difference in rotor diameter is due to a difference in hub geometry. A detailed description is given by Krogstad and Lund [24]. The turbine T3 is a downscaled version of turbine T1. Herein, the blade increment between the blade elements is halved, whereas twist and chord distribution are identical with the original. A more detailed description is given in Garica et al. [25]. All rotors are based on the airfoil NREL S826, which is described in detail in [26].

The measurements are conducted at two different ambient turbulence intensities, $I_a = 0.23\,\%$ and $10\,\%$. The low ambient turbulence intensity is reached in the clean wind tunnel without any flow disturbance. Furthermore, it can be considered as constant at all downstream distances. Note that an ambient turbulence intensity of $0.23\,\%$ can only occur in wind tunnel facilities. Therefore it is not applicable or comparable to full-scale wind turbine measurements or simulations. The high ambient turbulence intensity at turbine position is achieved by installing a turbulence grid at the inlet to the test section, as seen in Figure 1. By using the turbulence grid a turbulent flow is generated, which decays with downstream distance. Therefore, the ambient turbulence intensity amounts $5\,\%$ at $x/D = 3$, $4.1\,\%$ at $x/D = 5$ and eventually $3\,\%$ at $x/D = 9$. Note that these values apply to turbine T1. Using a different rotor diameter results in different ambient turbulence intensities at normalized downstream distances. According to WindPRO an ambient turbulence intensity of $10\,\%$ represents mixed water and land terrain [27]. Measured average values at offshore wind farms are $5.6\,\%$ at Lillegrund and $7\,\%$ at Horns Rev [8].

For the wake measurements a two-component laser doppler anemometry (LDA) is utilised. It measures mean and fluctuating velocities over a time series of 50 000 samples. All line wakes are measured at hub height in spanwise horizontal direction at a fixed downstream position. They consists of 40 measurement points between $-1 \leq z/D \leq 1$ using Turbine T1 and 25 measurement points between $-1.2 \leq z/D \leq 1.2$ using Turbine T3. All full wakes comprises 360 measurements points in vertical (y) and horizontal (z) direction at a fixed downstream (x) position in the range of $-0.8 \leq z/D \leq 0.8$ and $-0.8 \leq y/D \leq 0.8$. The reference velocity U_{ref} at the test section inlet is determined by measuring the pressure difference at two

Table 1: Wind turbines description including rotor diameter, hub height and design tip speed ratio

Turbine	Rotor diameter	Hub height	Design tip speed ratio
T1	0.944 m	0.817 m	6.0
T2	0.894 m	0.817 m	6.0
T3	0.450 m	0.817 m	3.5

Figure 1: Experimental set up in the wind tunnel using turbines T1 (in front) and T2 (behind) [28]

defined cross sections in the tunnel for every measurement point. It is used for normalization of the wake velocity. During the measurements the reference velocity is kept constant at 11.5 m/s. Furthermore, air temperature as well as ambient pressure are measured consistently to compute the air density. In total, two comprehensive wake measurement series are conducted. Test case A represents wake measurements behind turbine T3 at all integer downstream distances in the range of $x/D = 2-15$, applying two different ambient turbulence intensities. Test case B describes wake measurements behind turbine T1 at downstream distances $x/D = 3, 5$ and 9 using three different upstream turbine blade pitch angles. An overview is given in Table 2.

In order to compute the mechanical power output, the wind turbine torque T and rotational speed n are measured continuously on the rotor shaft. For this purpose, a torque transducer to measure torque and an optical photo cell for rotational speed are utilised. Additionally, the thrust force F is measured using a six-component force balance. Consequently, power output and thrust force described as power and thrust coefficient are

$$C_\mathrm{P} = \frac{2P}{\rho A_0 U_\mathrm{ref}^3} = \frac{T n_\mathrm{rpm}}{15 \rho R_0^2 U_\mathrm{ref}^3}, \tag{2.1}$$

$$C_\mathrm{T} = \frac{2F}{\rho \pi R_0^2 U_\mathrm{ref}^2}. \tag{2.2}$$

Both equations apply to downstream and upstream turbine. Test case C describes performance measurements at both turbines, varying the upstream turbine blade pitch angle. Three pitch angles $\beta = 0°, 2°$ and $5°$ are investigated. Furthermore, the downstream turbine is located at downstream distances $x/D = 3, 5$ and 9. The ambient turbulence intensity is kept constant at $I_\mathrm{a} = 10\,\%$. An overview is given in Table 3.

2.2 Comparison methods

To assess the wake models ability to predict the measured wakes, two different methods are applied in this work: the mean absolute percentage error MAPE and the newly proposed available power percentage error APPE.

The mean absolute percentage error is a widely used error measure that compares measured and modelled variables and computes an absolute mean error in percent. A comprehensive comparison of different error measures by Hyndman et al. [29] found the MAPE to be the preferred method. It should only not be used for a series of very small denominators, which is not the case in this work. A perfect prediction yields a MAPE of 0 %. For its calculation all measured velocities U_m are compared to the predicted velocities U_p at the exact same location in horizontal (z) direction. The overline represents an average over all the data points. Subsequently, the MAPE can be calculated by the following equation

$$MAPE = \frac{\overline{|U_\mathrm{m} - U_\mathrm{p}|}}{|U_\mathrm{m}|} \cdot 100. \tag{2.3}$$

The available power percentage error is a newly developed method. It compares the measured and modelled available power in the wind for extraction by a downstream turbine. Consequently, this method perfectly evaluates the wake models suitability for wind farm wake modelling purposes. Furthermore, this method is also suitable for top-hat shape wake models, since they are solely aiming at predicting the available power in the wake. To compute the available power for a downstream turbine, at first the average velocity in the wake over all data points located between $-R_0 < z < R_0$ is calculated. Subsequently, the average velocity is cubed and the APPE computed as follows

$$APPE = \frac{\overline{U_\mathrm{m}^3} - \overline{U_\mathrm{p}^3}}{\overline{U_\mathrm{m}^3}} \cdot 100 \quad , -R_0 < z < R_0. \tag{2.4}$$

In contrast to the MAPE, the APPE can become negative, since no absolute velocities are used. A negative APPE represents an overestimation of the measured available power extractable for a downwind turbine. Therefore, a positive value describes an underestimation.

For performance comparison, the modelled thrust and power coefficients at operating tip speed ratio (TSR) are directly compared to the measured values. This applies to the upstream as well as the downstream turbine.

2.3 Blockage correction

In small-scale wind tunnel measurements a so-called blockage effect can be observed. The blockage effect describes the condition, in which air flow in the wind tunnel is partially blocked by the wind turbine rotor area. Consequently, the inflow velocity in blocked conditions is higher than in a non-blocked situation. Hence, the aim of blockage effect correction is to determine the corrected inflow velocity. For appropriate comparisons of wind tunnel measurements and open field measurements or simulations, a blockage effect correction is crucial. Particularly, for calculating the wind turbine power and thrust, which increases with the cube and square of the inflow velocity, respectively.

Blockage effect measurements conducted by Chen et al. [30] found the blockage effect to strongly depend on the rotor tip speed ratio λ, pitch angle β and the blockage ratio α. The blockage ratio is defined as the ratio between the rotor disk area A_0 and the wind tunnel cross section area A_T

$$\alpha = \frac{A_0}{A_\mathrm{T}}. \tag{2.5}$$

Table 2: Overview of wake measurement test cases

Test Case	Upstream Turbine	TSR [-]	Pitch [°]	I_a [%]	Downstream distance [D]
A	T3	3.5	0	0.23, 10	2 - 15
B	T1	6	0, 2, 5	10	3, 5, 9

Table 3: Overview of performance measurement test cases with $I_a = 10\,\%$

Test Case	Upstream Turbine	TSR [-]	Pitch [°]	Downstream turbine	Downstream distance [D]
C	T1	6	0, 2, 5	T2	3, 5, 9

Considering the wind tunnel cross section area from section 2.1 this results in 14.3 % for turbine T1, 12.8 % for T2 and 3.2 % for T3. Since tip speed ratio as well as pitch angle variation influence the rotor thrust, the blockage effect correction can be described as a function of blockage ratio and rotor thrust.

In the present study the blockage effect correction method proposed by Ryi et al. [2] based on the one-dimensional momentum approach of Glauert is used. By applying one-dimensional axial momentum theory and various assumptions, a set of six equations can be derived. Knowing the blockage ratio and measuring or simulating the thrust, six unknowns remain. Since the corrected velocity is one of those unknowns, it can easily be computed. The detailed derivation of the applied correction method can be found in A.1.

If one wants to compare full-scale turbine simulations with small-scale turbine wind tunnel measurements, the following correction of power coefficient, thrust coefficient and tip speed ratio has to be applied. Note that in this work the modelled and not the measured values are corrected

$$C_{\mathrm{P,cor}} = C_{\mathrm{P}} \left(\frac{U_{\mathrm{cor}}}{U_{\mathrm{ref}}} \right)^3, \tag{2.6}$$

$$C_{\mathrm{T,cor}} = C_{\mathrm{T}} \left(\frac{U_{\mathrm{cor}}}{U_{\mathrm{ref}}} \right)^2, \tag{2.7}$$

$$\lambda_{\mathrm{cor}} = \lambda \left(\frac{U_{\mathrm{cor}}}{U_{\mathrm{ref}}} \right), \tag{2.8}$$

where $U_{\mathrm{cor}}/U_{\mathrm{ref}}$ is the blockage effect correction factor. A blockage effect correction is necessary for the upstream as well as the downstream turbine. Additionally, a blockage effect correction is used to correct the wake velocities computed by the wake models, which are described inn the next section

$$U_{\mathrm{cor}} = U \left(\frac{U_{\mathrm{cor}}}{U_{\mathrm{ref}}} \right). \tag{2.9}$$

The normalized corrected inflow velocities for Turbines T1, T2 and T3 are displayed as a function of the thrust coefficient C_{T} in Figure 2.

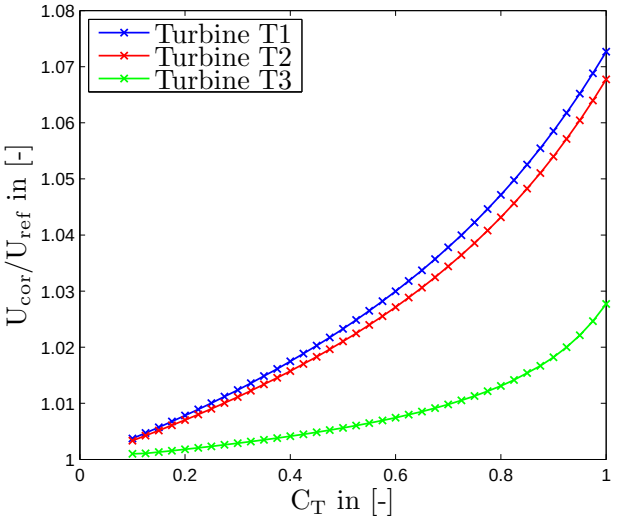

Figure 2: Blockage effect correction results as a function of thrust coefficient for all turbines

2.4 Wake models

Jensen model

The Jensen wake model is based on conservation of momentum. It further assumes a uniform velocity profile and a linear expanding wake. The normalized wake velocity and wake width as a function of downstream distance x are

$$\frac{U(x)}{U_{\mathrm{ref}}} = 1 - \frac{1 - \sqrt{1 - C_{\mathrm{T}}}}{(1 + 2kx/D_0)^2} \tag{2.10}$$

and

$$D_{\mathrm{w}}(x) = 2kx + D_0, \tag{2.11}$$

where k is the wake decay constant. The constant basically describes the slope of the wake expansion. According to N.O. Jensen this value is constant and approximately 0.1 [13]. However, detailed subsequent investigations found the wake decay constant to be a function of surface roughness and thus the ambient turbulence intensity [27] [31] [32]. Various equations exist in order to calculate or estimate the wake decay coefficient. In this work the widely used correlation

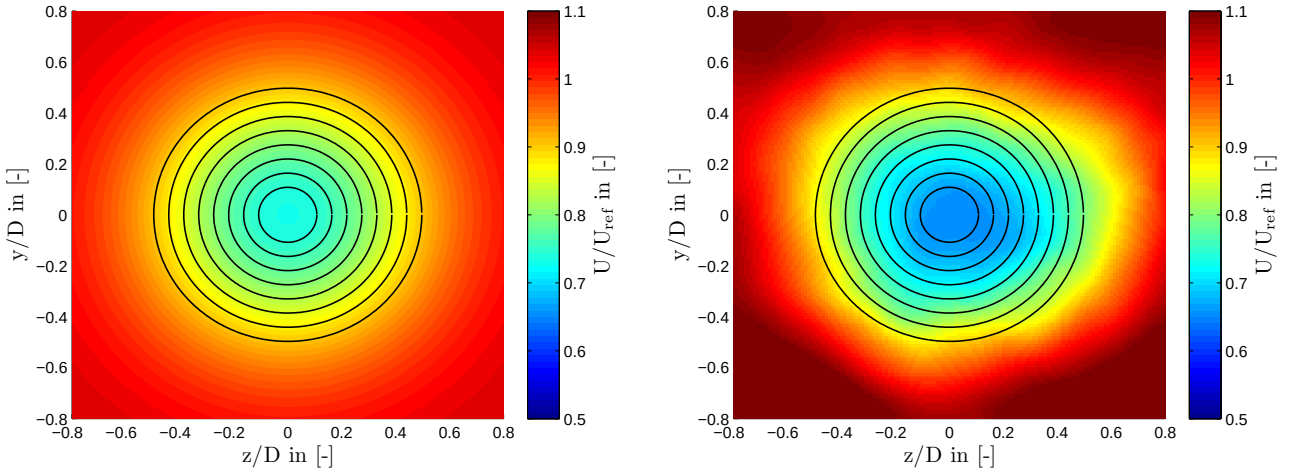

Figure 3: Blade elements of a turbine located in the **(left:)** modelled fullwake using the adjusted Jensen-Gaussian wake model and blockage effect correction and **(right:)** measured fullwake at $x/D = 6$ and $I_\mathrm{a} = 10\,\%$

from WindPRO is applied [32]

$$k \approx 0.5 I_\mathrm{a}. \tag{2.12}$$

Larsen model

The 2009 version of the Larsen model is based on Prandtl's turbulent boundary layer equations. The model is further based on a closed-form solution to the Reynolds-Averaged Navier Stokes (RANS) and assumes a self-similar velocity profile. Moreover the flow is assumed to be incompressible, stationary and due to neglection of wind shear, axisymmetric. Larsen solved the RANS equations by using a first order approximation together with continuity equation. Compared to the earlier version, Larsen defines two boundary conditions, which he found empirically from full-scale turbine measurements. Neglecting the second order approximation, the normalized velocity profile in axial and radial direction

$$\frac{U(x,r)}{U_\mathrm{ref}} = 1 - \frac{1}{9}\left(C_\mathrm{T} A_0 \left(x + x_0\right)^{-2}\right)^{\frac{1}{3}} \left(r^{\frac{3}{2}}\left(3c_1^2 C_\mathrm{T} A_0 \left(x + x_0\right)\right)^{-\frac{1}{2}} - \left(\frac{35}{2\pi}\right)^{\frac{3}{10}} \left(3c_1^2\right)^{-\frac{1}{5}}\right)^2, \tag{2.13}$$

and the wake radius are

$$R_\mathrm{w}(x) = \left(\frac{105 c_1^2}{2\pi}\right)^{\frac{1}{5}} \left(C_\mathrm{T} A_0 \left(x + x_0\right)\right)^{\frac{1}{3}}, \tag{2.14}$$

where $c1$ and x_0 are parameters, which are defined in A.2.

Ishihara model

The Ishihara model is based on momentum conservation, a two-dimensional axisymmetric flow and a self-similar wake. It further takes the influence of ambient and rotor added turbulence intensity on the wake recovery into account. Hence, the wake velocity as well as the wake width b are depending on the rate of wake recovery p, which in turn is a function of turbulence intensity. The normalized velocity and the wake width are given by

$$\frac{U(x,r)}{U_\mathrm{ref}} = \frac{C_\mathrm{T}^{0.5}}{32}\left(\frac{1.666}{k_1}\right)^2 \left(\frac{x}{D_0}\right)^{-p} \exp\left(-\frac{r^2}{b^2}\right), \tag{2.15}$$

$$b(x) = \frac{k_1 C_\mathrm{T}^{0.25}}{0.833} D_0^{1-\frac{p}{2}} x^{\frac{p}{2}}, \tag{2.16}$$

with

$$p = k_2 \left(I_\mathrm{a} + I_\mathrm{wake}\right) \tag{2.17}$$

and

$$I_\mathrm{w} = \begin{cases} k_3 \frac{C_\mathrm{T}}{I_\mathrm{a}} \left(1 - \exp\left(-4\left(\frac{x}{10 D_0}\right)^2\right)\right) & , I_\mathrm{a} > 0.03 \\ k_3 \frac{C_\mathrm{T}}{0.03} \left(1 - \exp\left(-4\left(\frac{x}{10 D_0}\right)^2\right)\right) & , I_\mathrm{a} \leq 0.03. \end{cases}$$

Frandsen model

Frandsen derived his model by applying mass and momentum conservation to a control volume around the turbine. Same as the Jensen wake model, it further assumes a uniform velocity profile inside the wake. The velocity profile and the wake diameter can be described by

$$\frac{U(x)}{U_\mathrm{ref}} = 1 - \left(\frac{1}{2}\left(1 - \sqrt{1 - 2\frac{A_0}{A_\mathrm{w}} C_\mathrm{T}}\right)\right), \tag{2.18}$$

$$D_\mathrm{w}(x) = \left(\beta + \frac{\alpha x}{D_0}\right)^{\frac{1}{2}} D_0, \tag{2.19}$$

with

$$\beta = \frac{1 + \sqrt{1 - C_\mathrm{T}}}{2\sqrt{1 - C_\mathrm{T}}}. \tag{2.20}$$

Consequently, the initial wake diameter is $D_\mathrm{w}(x = 0) = \sqrt{\beta} D_0$. Due to $\beta > 1$ this assumption is not realistic, but ensures a solution for all values of the thrust coefficient between 0 and 1. Furthermore, the

expansion factor α can be expressed as a function of the wake decay constant and is in order of $\alpha = 10k$.

Bastankah & Porté-Agel model

The wake model is derived by applying mass and momentum conservation. Additionally, viscous and pressure terms are neglected in the momentum equation and a self-similar wake with Gaussian shape is assumed. Similar to the Jensen model the wake is expected to expand linearly with a growth rate k^*. The resulting equation for the normalized wake velocity as a function of the streamwise and spanwise directions x, y, z is

$$\frac{U(x,y,z)}{U_{\text{ref}}} = 1 - \left(1 - \sqrt{1 - \frac{C_{\text{T}}}{8\left(k^* x/D_0 + \epsilon\right)^2}}\right) \exp\left(\frac{-1}{2\left(k^* x/D_0 + \epsilon\right)^2}\left(\frac{z - z_{\text{h}}}{D_0}\right)^2 + \left(\frac{y}{D_0}\right)^2\right). \tag{2.21}$$

Large Eddy Simulations (LES) found the value of ϵ to be

$$\epsilon = 0.2\sqrt{\beta}. \tag{2.22}$$

Subsequently, based on LES results Niayfar & Porté-Agel [7] found the following empirical expression for the wake growth rate

$$k^* = 0.3837I + 0.003678, \tag{2.23}$$

applicable in the range of $6.5\,\% < I < 15\,\%$, where I is the local streamwise turbulence intensity immediately upwind of the rotor center. Note that (2.23) is used for wind farm calculations. In case of a single wake the turbulence intensity immediately upwind of the rotor equals the ambient turbulence intensity $I = I_{\text{a}}$.

Jensen-Gaussian wake model

The Jensen-Gaussian wake model (JGWM) combines the Jensen model velocity deficit calculation with an Gaussian wake shape. Based on three assumptions, (i) JGWM and Jensen model have the same wake radius, (ii) immediately outside of the wake region the velocity equals the freestream velocity U_{ref} and (iii) across the wake both models have the same mass flow flux, the normalized velocity can be calculated as follows

$$\frac{U(x,r)}{U_{\text{ref}}} = 1 - \left(1 - U_{\text{c}}(x)\right)\frac{5.16}{\sqrt{2\pi}} \exp\left(\frac{-r^2}{\left(k'x + R_0\right)^2/3.3282}\right). \tag{2.24}$$

The centerline velocity U_{c} is equal to the one computed by the Jensen model (2.10).

$$U_{\text{c}}(x) = 1 - \frac{1 - \sqrt{1 - C_{\text{T}}}}{\left(1 + 2k'x/D_0\right)^2}, \tag{2.10}$$

where k' is the modified wake decay constant. Compared to the standard wake decay constant the modified constant is a function of the ambient and the rotor added turbulence intensity. Tian et al. [33] proposed the following correlation between those two coefficients

$$k' = k\frac{I_{\text{wake}}}{I_{\text{a}}}. \tag{2.25}$$

Gao et al. proposed an own empirical engineering model to compute the turbulence intensity I_{wake} inside the wake. In this work, the Gao turbulence model combined with the above mentioned wake model, will be referred to as the original Jensen-Gaussian wake model

$$I_{\text{wake,Gao}} = \left(0.4\frac{C_{\text{T}}}{\left(x/D_0\right)^{0.5}} + I_{\text{a}}^{0.5}\right)^2. \tag{2.26}$$

In addition, other turbulence intensity models could be used in combination with the wake model. Such as the Tian turbulence model [33]

$$I_{\text{wake,Tian}} = 0.4\frac{C_{\text{T}}}{x/D_0} + I_{\text{a}}, \tag{2.27}$$

the Frandsen turbulence model [34]

$$I_{\text{wake,Frandsen}} = \sqrt{0.4\frac{C_{\text{T}}}{\left(x/D_0\right)^2} + I_{\text{a}}^2}, \tag{2.28}$$

the Crespo and Hernandez turbulence model [35] for parameter ranges $5 < x/D < 15$, $7\,\% < I_{\text{a}} < 15\,\%$ and $0.1 < a < 0.4$, with $a = 0.5\left(1 - \sqrt{1 - C_{\text{T}}}\right)$

$$I_{+,\text{C\&H}} = 0.73a^{0.8325} I_{\text{a}}^{0.0325} \left(x/D_0\right)^{-0.32}, \tag{2.29}$$

where I_+ is the rotor added turbulence intensity and a is the axial induction factor. Moreover, the Hassan and Hassan turbulence model [36]

$$I_{+,\text{H\&H}} = 5.7C_{\text{T}}^{0.7} I_{\text{a}}^{0.68} \left(x/D_0\right)^{-0.96}, \tag{2.30}$$

where x_{n} is the near wake length, which is derived in section A.3. Eventually, the Quarton and Ainslie turbulence model [37]

$$I_{+,\text{Q\&A}} = 4.8C_{\text{T}}^{0.7} I_{\text{a}}^{0.68} \left(x/D_0\right)^{-0.57}. \tag{2.31}$$

All rotor added turbulence models use the following equation to compute the turbulence intensity inside the wake

$$I_{\text{wake}} = \sqrt{I_{\text{a}}^2 + I_{+}^2}. \tag{2.32}$$

2.5 Blade Element Momentum method

In order to model power output and thrust force of the upstream and downstream turbine a Blade Element Momentum method is used. Furthermore, a mean-blade-element-velocity method is presented to handle the non-uniform inflow velocity for the downstream

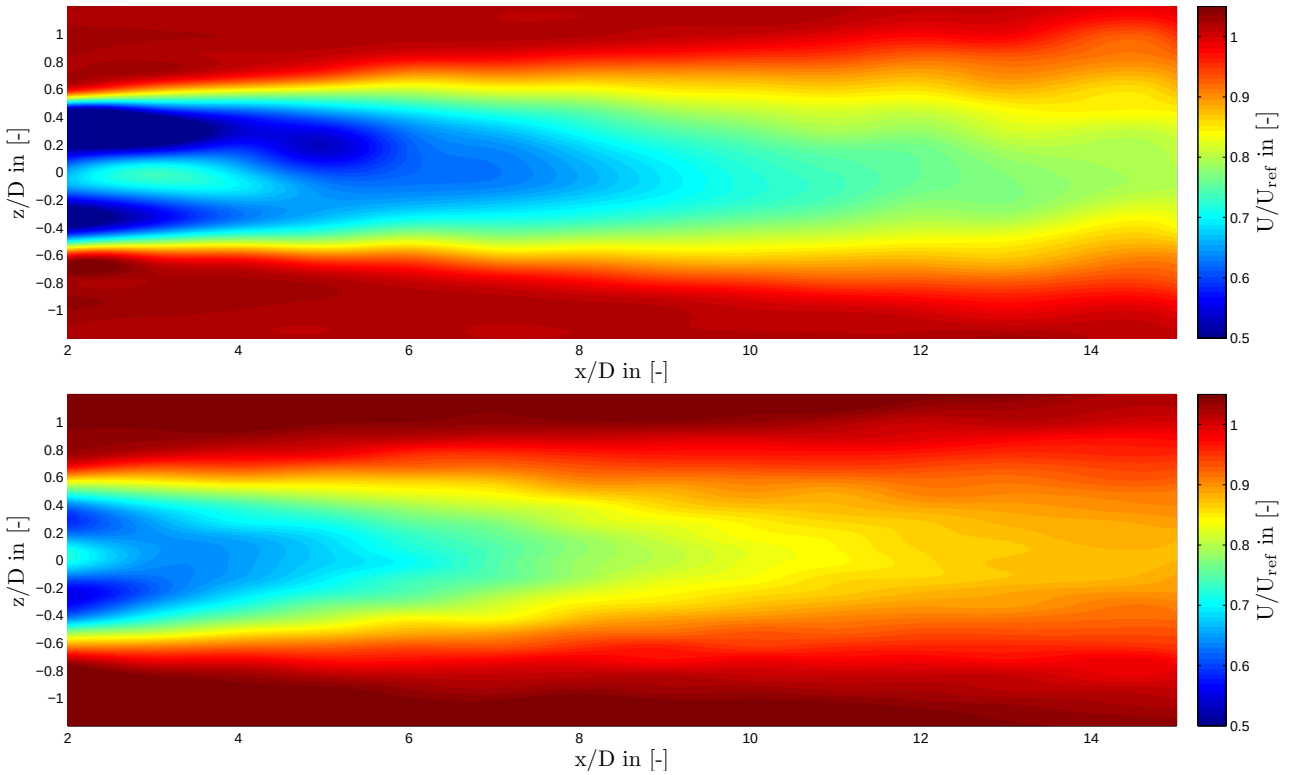

Figure 4: Test case A: Wake measurement results at hub height at **(top:)** low ambient turbulence intensity $I_a = 0.23\,\%$, **(bottom:)** high ambient turbulence intensity $I_a = 10\,\%$ at downstream distances $x/D = 2 - 15$

turbine located in the wake. In this section, the robust and efficient BEM solution method with guaranteed convergence by S.Ning [1] is briefly described. In A.4 the method is derived in detail.

In classical solution methods the BEM equations are a function of two variables, the axial and tangential induction factor a and a'. They are solved through an iterative approach, which often leads to convergence problems. In order to overcome convergence problems, S. Ning proposed to reduce the two equations from classical BEM theory into one equation parametrized by only one variable, the local inflow angle ϕ. Consequently, it is possible to apply a one-dimensional root-finding algorithm. In his work S.Ning proofed that a suitable algorithm, like Brent's method [38], always converges. Further benefits are the very high robustness and high efficiency in terms of computational time.

Additionally, the applied method includes Prandtl's tip loss factor, which serves to correct the assumption of an infinite number of blades from classical BEM theory [21]. Furthermore, the hub-loss factor corrects the induced velocity resulting from a vortex being shed near the hub of the rotor [39]. For high axial induction factors the momentum theory is invalid. Therefore, empirical equations have to be applied instead. In this work Buhl's correction method [40] is used. Finally, the induction factors are used to compute the induced velocity and thus the Reynolds number. This is only necessary, if Reynolds number dependence is included when modelling lift and drag forces on the airfoil.

In order to model the downstream turbine performance the simulated wake velocities from the analytical models are used. Figure 3 shows an example of a modelled wake using the Jensen-Gaussian wake model, where the rotor is divided into 7 blade elements. Instead of using one inflow wind speed for all blade elements, a mean velocity for each blade element is calculated. Subsequently, this mean velocity is used as the inflow wind speed for that specific blade element. The method is called mean-blade-element-velocity method. An alternative is a simple velocity averaging over the rotor swept area, herein called mean-rotor-velocity method. Both methods will be applied and compared in section 3.2.2.

3 Results and discussion

3.1 Wake prediction

In the following section, the wake measurements are compared to the predicted wakes by the wake models. This is done separately for each test case. For an evaluation of the wake characteristics, the parameters near wake length, wake recovery and wake expansion are utilised. At first, the measurement results are presented and discussed. Subsequently, the modelling results of each wake model are compared to the measurements.

Table 4: Test case A: Wake prediction results using the comparison methods MAPE and absolute APPE averaged over downstream distances $x/D = 2 - 15$ at two ambient turbulence intensities

	$I_a = 0.23\,\%$		$I_a = 10\,\%$	
	MAPE [%]	APPE [%]	MAPE [%]	APPE [%]
Jensen	19.6	84.7	6.8	6.7
Larsen	9.8	39.4	8.6	51.7
Frandsen	8.4	29.5	10.3	60.1
Ishihara	7.3	28.9	3.8	6.5
BP	-	-	5.3	20.2
JGWM	5.16	11.2	3.4	3.3

3.1.1 Test Case A

Test case A describes a variation of the ambient turbulence intensity, while the blade pitch angle is kept constant at $\beta = 0°$. Wake measurements at two ambient turbulence intensities, $I_a = 0.23\,\%$ and $I_a = 10\,\%$ are conducted. Additional thrust measurements yield a thrust coefficient of 0.8847 at design TSR. This value will be applied as input parameter to the wake models. Using turbine T3 and the measured thrust coefficient results in a blockage effect correction factor of 1.0173. The measurement results are given in Figure 4 in a two dimensional XZ-Plot. For this measurement 25 points in horizontal direction at 14 downstream positions are measured, which yields 375 measurement points. A two dimensional spline interpolation is applied to compute the approximate values in between. The corresponding measured and predicted line wakes are given in Figure 7 and Figure 8. Furthermore, the half-width wake $b_{1/2}$ is displayed in Figure 5. For evaluation of the wake model prediction accuracy the comparison methods MAPE and APPE are used. The absolute averaged values over all downstream distances are given in Table 4. In addition, all wake model XZ-Plots and comparison method results separated at all downstream distances are given in the appendix.

From Figure 7 and Figure 8 a near wake length of roughly $x/D = 5$ at $I_a = 0.23\,\%$ and $x/D = 3$ at $I_a = 10\,\%$ can be determined. Note that in this work the near wake is defined as the area behind the rotor, where a double-Gaussian wake shape is maintained [4]. This observation is in accordance with theory, where the near wake length is found to be proportional to ambient turbulence intensity [4] [41]. Additionally, an asymmetry in the near wake can be observed at both ambient turbulence intensities. The effect is caused by the interference of the wake caused by the turbine tower [42]. From downstream distances of about $x/D = 6$ at $I_a = 0.23\,\%$ and $x/D = 4$ at $I_a = 10\,\%$ the wake shows the typical single-Gaussian wake shape. According to the above mentioned definition this region is therefore defined as the far wake.

In Figure 4 the increase of the wake velocity with downstream distance, defined as wake recovery, can be clearly observed. The wake recovery is significantly higher in case of high ambient turbulence intensity. This is in accordance with literature [27] and full-scale measurements conducted by Baker and Walker [43], where a slower wake recovery at low ambient turbulence levels was observed. To underline the influence of ambient turbulence intensity on a wind turbine power output, a comparison at $x/D = 6$ is made in the following. At $I_a = 0.23\,\%$ the average normalized wake velocity over the rotor swept area amounts 0.662, whereas it is 0.762 at $I_a = 10\,\%$. This is equivalent to a percentage difference in wind power ($P = 0.5\rho AU^3$) of 41.6 %, which is significant. However, at this point the reader should be reminded that an ambient turbulence intensity of 0.23 % is not realistic and only occurs in a laboratory environment.

In Figure 5 the measured and modelled half-width wakes $b_{1/2}$ are plotted over the downstream distance x at both ambient turbulence intensities. Furthermore, the regression curves are displayed. In this work the wake width b is defined at $U/U_{\mathrm{ref}} = 1$. Consequently, the half-width wake is wake width divided by two. At $I_a = 0.23\,\%$ the wake expansion is evidently linear. Therefore, the measured wake decay constant k can be calculated easily by determining the slope. The resulting wake decay constant amounts $k = 0.0372$. At $I_a = 10\,\%$ the wake expansion is square-shaped. This is probably caused by the decay of ambient turbulence intensity with downstream distance, as described in section 2.1. In order to verify this assumption additional measurements or CFD simulations with constant ambient turbulence intensities are necessary. Moreover, comparing the measured half-width wake at both ambient turbulence intensities, a higher wake expansion at $I_a = 0.23\,\%$ from $x/D = 10$ can be observed. This observation is not at all in accordance with literature, where the wake expansion was found to be proportional to the ambient turbulence intensity [31] [32]. However, inserting (2.12) and (2.25) in (2.32) yields

$$k' = 0.5\sqrt{I_a^2 + I_+^2}. \tag{3.1}$$

Consequently, the modified wake decay constant can be regarded as a function of ambient turbulence intensity and rotor added turbulence intensity. The mea-

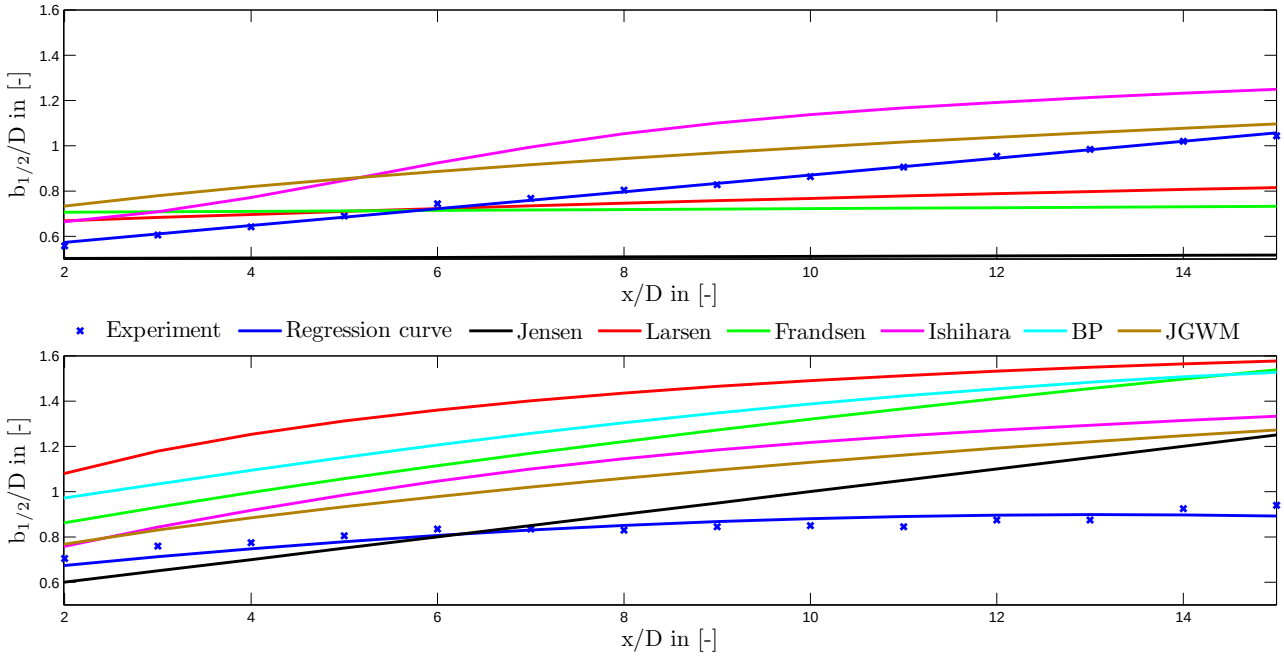

Figure 5: Test case A: Half-width wake measurement and modelling comparison at hub height at **(top:)** low ambient turbulence intensity $I_a = 0.23\,\%$, **(bottom:)** high ambient turbulence intensity $I_a = 10\,\%$ at downstream distances $x/D = 2 - 15$

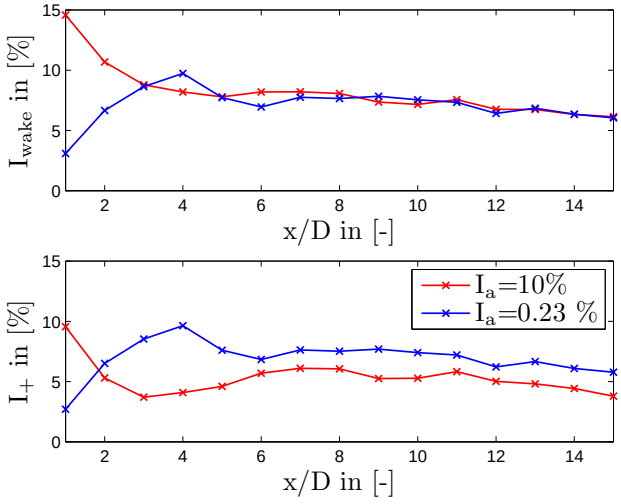

Figure 6: Test case A: Measured wake turbulence intensity I_{wake} at centerline and calculated rotor added turbulence intensity I_+ at both ambient turbulence intensities

sured wake turbulence intensity I_{wake} at centerline and the calculated rotor added turbulence intensity I_+ using (2.32) are displayed in Figure 6 at both ambient turbulence intensities. Apparently, the wake turbulence intensities are almost identical from $x/D = 3$. Consequently, the rotor added turbulence intensity has to be higher in case of low ambient turbulence intensity. Therefore, the rotor added turbulence intensity could have a stronger influence on wake expansion than commonly assumed. However, more detailed investigations are necessary in order to potentially verify this assumption.

Since all models are incapable of predicting the double-Gaussian wake shape, the near wake length can not be modelled. Furthermore, the wake models are unable to model the tower influence in the near wake. However, this is not necessary for wind farm applications, where turbine spacing is generally between 4 and 8 rotor diameters [9]. Moreover, analytical wake models aim at predicting a wind farm power output. Hence, the available power in the wind is more important than the actual wake shape.

At $I_a = 0.23\,\%$ the **Jensen model** underestimates the wake velocity significantly at all downstream distances. The model almost shows no wake recovery at all. As an example, at $x/D = 2$ the normalized centerline velocity amounts about 0.35, whereas it is 0.39 at $x/D = 15$. Same applies to the half-width wake, which is strongly underestimated at all downstream distances and almost not increases at all. Consequently, this results in a high percentage error in MAPE and APPE of 19.6 % and 84.7 %, respectively. This represents the highest prediction error among all wake models. The strong underestimation of wake recovery and wake expansion is caused by the small wake decay constant of 0.0012, calculated using equation (2.12). In WindPRO [27] the smallest recommended wake decay constant is 0.04 at offshore terrain and an ambient turbulence intensity of 8 %. Therefore, the Jensen model is simply not applicable at ambient turbulence intensities lower than 8 %. At $I_a = 10\,\%$ the Jensen wake model performs significantly better. Even though the centerline velocity is slightly overestimated from $x/D = 3$, the model yields an average APPE of only 6.7 % due

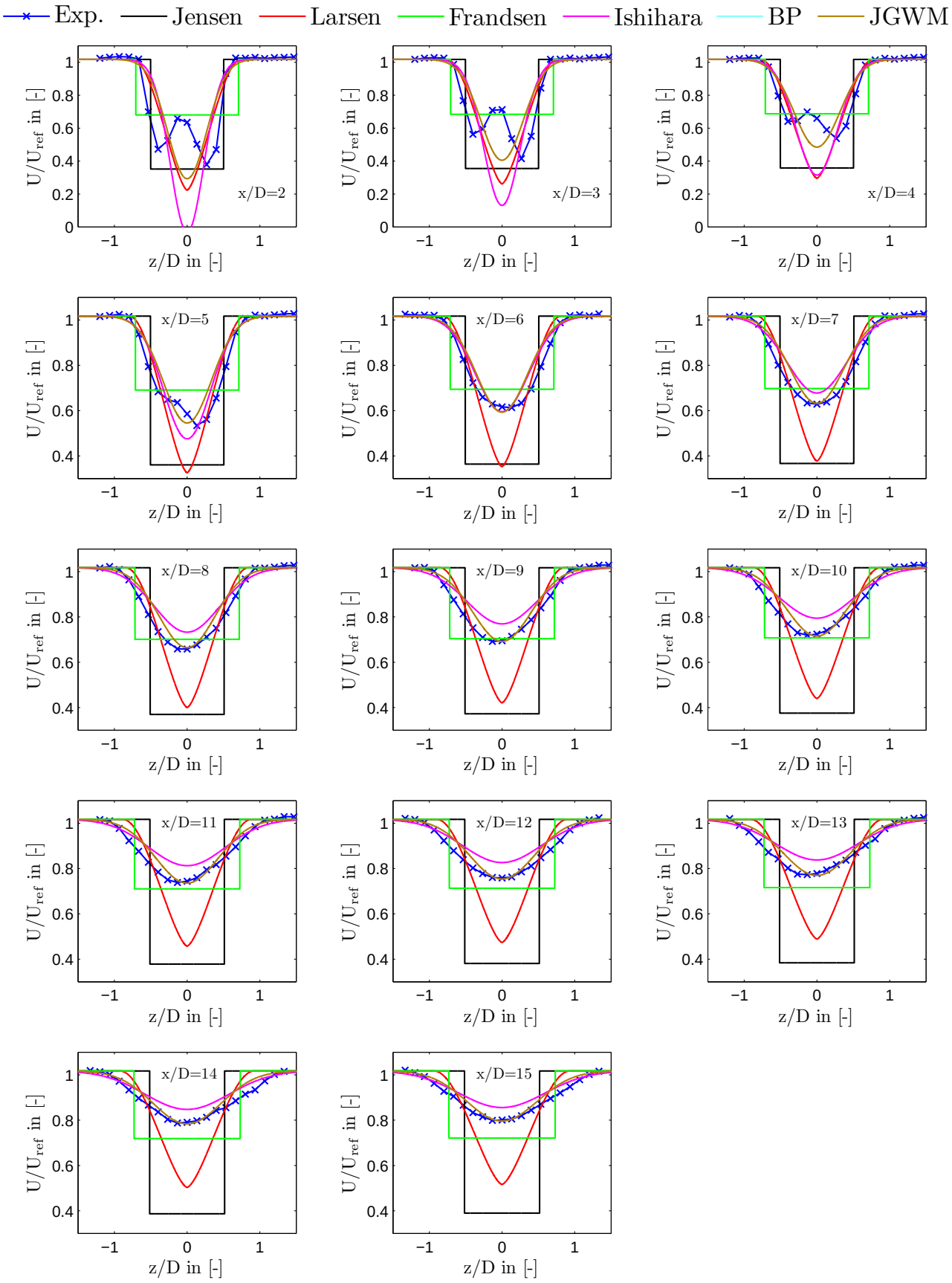

Figure 7: Test case A: Wake measurement and modelling comparison at hub height at $I_a = 0.23\,\%$ and downstream distances $x/D = 2 - 15$

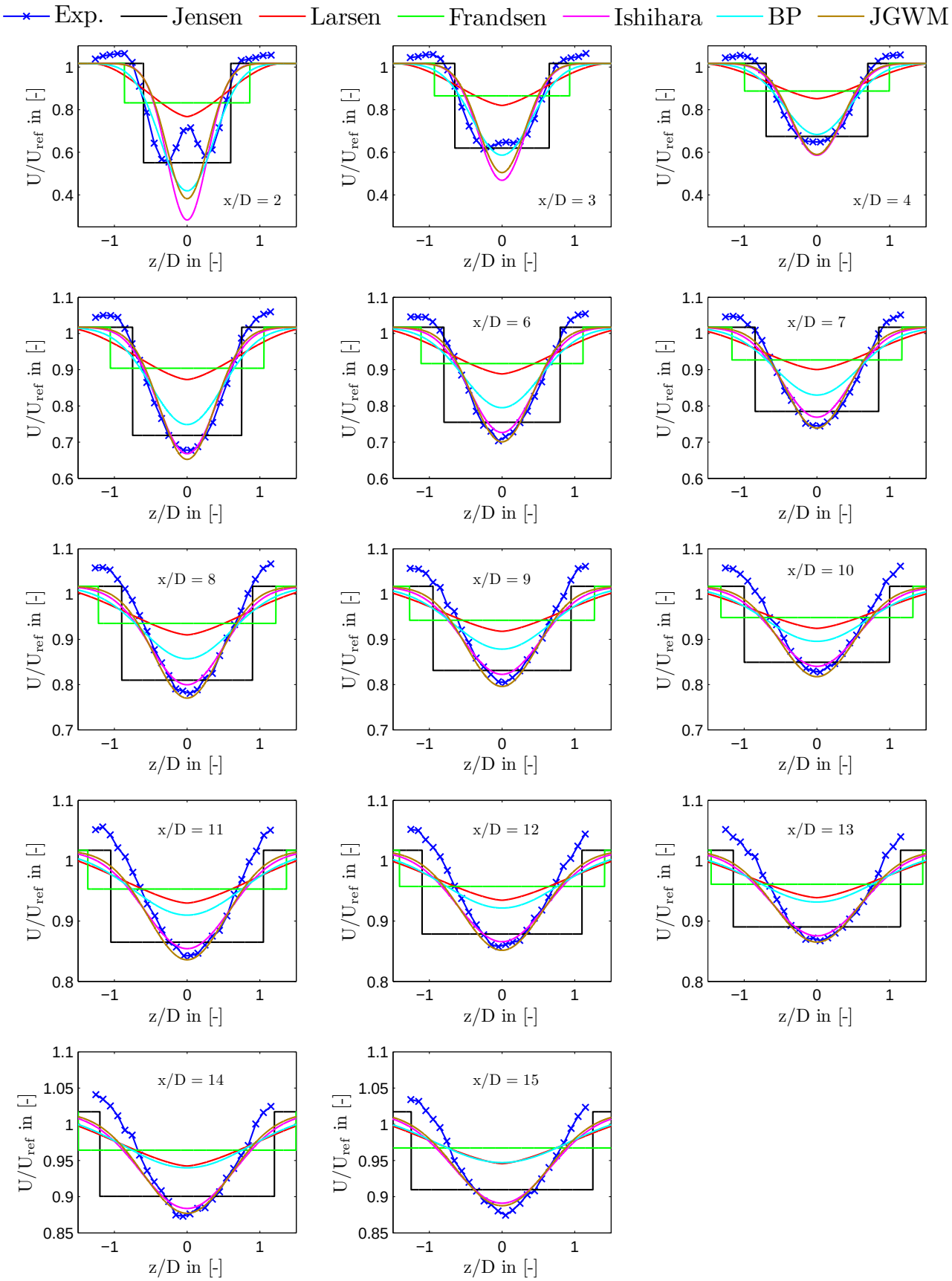

Figure 8: Test case A: Wake measurement and modelling comparison at hub height at $I_a = 10\,\%$ and downstream distances $x/D = 2 - 15$

to the top-hat wake shape. Considering only the far wake, an APPE of only 3.2 % is achieved. Moreover, the Jensen model gives the best half-width wake prediction among all models. However, at downstream distances from $x/D = 10$ the wake expansion is still strongly overestimated. Assumingly, this is caused by the ambient turbulence intensity decay in the wind tunnel, which is not taken into account by the wake models.

The **Larsen model** shows a very high sensitivity regarding ambient turbulence intensity. Therefore, the model shows opposed predictions results. At $I_a = 0.23\,\%$ the wake velocity is underestimated at all downstream distances. However, the half-width wake is reasonable predicted and only shows a significant deviation from about $x/D = 10$. Nevertheless, a MAPE of 9.8 % and APPE of 39.4 % represents a very inaccurate prediction. Conversely, at $I_a = 10\,\%$ the wake velocity is overestimated at all downstream distances. Furthermore, the model strongly overestimates the half-width wake. Consequently, the prediction errors MAPE and APPE of 8.6 % and 51.7 %, respectively, represent a very high prediction inaccuracy. Hence, the Larsen model only seems to be applicable at lower ambient turbulence intensities approximately up to 6 %. These observations are in accordance with full-scale turbine wake comparisons at Horns Rev and Lillegrund [8].

The **Frandsen model** is characterized by a high wake velocity immediately behind the rotor as well as a low wake recovery rate, independent on the ambient turbulence intensity. At $I_a = 0.23\,\%$ the normalized centerline velocity recovers from 0.68 at $x/D = 2$ to only 0.72 at $x/D = 15$. In addition, almost no wake expansion occurs. At $I_a = 10\,\%$ the centerline velocity is significantly overestimated at all downstream distances. Same applies to the wake expansion. Therefore, all comparison methods represent a very low prediction accuracy at both ambient turbulence intensities. This observation is in accordance with full-scale turbine LES comparisons at different surface roughnesses [19].

The **Ishihara model** represents a good overall prediction accuracy. At $I_a = 0.23\,\%$ the centerline velocity, particularly in the far wake, shows reasonable agreement with the measurement. However, the wake width is overestimated over the entire downstream distances. In total, a MAPE of 7.3 % and APPE of 28.9 % represent rather an inaccurate prediction. However, at $I_a = 10\,\%$ the model shows very good agreement with the measurement. Particularly, in the far wake from $x/D = 4$ the centerline velocity is almost perfectly modelled. Conversely, the wake expansion is overestimated at all downstream distances. Again, this is most likely due to the ambient turbulence intensity decay in the wind tunnel. However, an average MAPE of 3.8 % and APPE of 6.5 % represent a very good prediction accuracy. Regarding only the far wake those values change to 2.6 % and 3.2 %, respectively.

Since, the **BP model** is only defined at ambient turbulence intensities between 6.5 % and 15 %, there are no results at $I_a = 0.23\,\%$. Even though the range appears to be small, it covers all offshore and most onshore applications according to WindPRO [27]. At $I_a = 10\,\%$ the wake velocity prediction is characterized by a strong overestimation from $x/D = 4$. The same overestimation applies to the wake expansion. Therefore, the model only yields an APPE of 20 %, which represents a rather inaccurate wake prediction.

The original **Jensen-Gaussian wake model** gives a very inaccurate prediction at $I_a = 0.23\,\%$. The prediction is characterized by a strong underestimation of the wake velocity. As an example, the normalized centerline velocity at $x/D = 15$ amounts only 0.19. Similar applies to the half-width wake, which is underestimated at all downwind distances. Consequently, a very low prediction accuracy is achieved. Conversely, at $I_a = 10\,\%$ the wake flow is well predicted. Only a slight overestimation of centerline velocity and thus available power occurs. Therefore, the average APPE amounts roughly 9 %. However, further investigations of the JGWM found a strong sensitivity to the applied turbulence intensity model. Therefore, using another turbulence model than the Gao model results in a significantly different wake prediction. Applying the Crespo and Hernandez turbulence model improves the wake flow prediction noticeable. That applies to centerline velocity as well as wake expansion at both ambient turbulence intensity. Consequently, at $I_a = 0.23\,\%$ the average MAPE amounts 5.2 % and APPE 11.2 %. This represents by far the best prediction results at low ambient turbulence intensity. Moreover, at $I_a = 10\,\%$ a MAPE of only 3.4 % and APPE of only 3.3 % are achieved. Again, this represents the best wake flow prediction. Consequently, the JGWM model in combination with the Crespo and Hernandez turbulence model will be used in the following. It will further be referred to as the adjusted JGWM. Note that in Table 4, Figure 5, Figure 7, and Figure 8 the turbulence-adjusted wake model is already displayed.

3.1.2 Test Case B

Test case B describes a variation of the blade pitch angle, while the ambient turbulence intensity is kept constant at 10 %. Wake measurements at three pitch angles $\beta = 0°$, 2° and 5° are conducted using Turbine T1. The associated thrust coefficients determined by measurements are 0.8497, 0.6944 and 0.517, respectively. The resulting blockage correction factors are 1.0525, 1.0373 and 1.0243. The measurement and modelling results are given in Figure 9 as line wakes at $x/D = 3, 5$ and 9.

Increasing the blade pitch angle away from the design point $\beta = 0°$ reduces the angle of attack. Therefore, the blade lift decreases, whereas the drag increases. Consequently, the power output and rotor thrust decrease, which results in a higher wake velocity behind

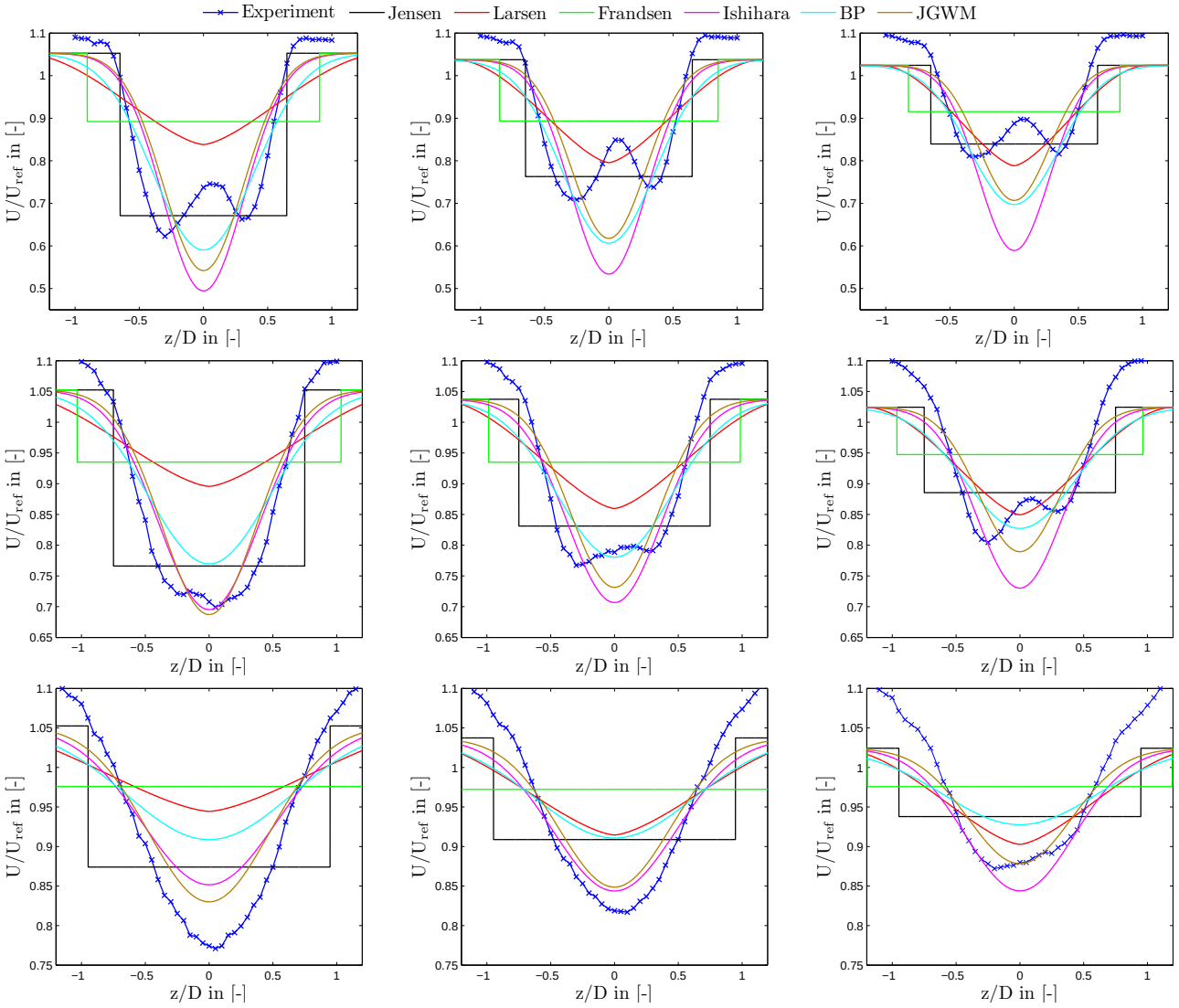

Figure 9: Test case B: Wake measurement and modelling comparison at hub height at three pitch angles **(left column:)** $\beta = 0°$, **(center column:)** $\beta = 2°$, **(right column:)** $\beta = 5°$ at downstream distance **(top row:)** $x/D = 3$, **(center row:)** $x/D = 5$, **(bottom row:)**$x/D = 9$

the turbine. This can be confirmed by the measurement results. At $x/D = 3$ the minimum wake velocity amounts 0.62 at 0°, whereas it is 0.71 and 0.81 at 2° and 5°, respectively. A similar wake velocity increase with increasing pitch angle can be observed at $x/D = 5$ and $x/D = 9$. Furthermore, the measurements at $x/D = 5$ reveal a double-Gaussian wake shape at $\beta = 2°$ and 5°. Whereas, the near wake length at $I_a = 10\,\%$ was earlier found to be in order of 3 to 4 rotor diameters. Consequently, one could assume that the near wake length increases with increasing pitch angle. Therefore, the near wake length is inversely proportional to the thrust coefficient. This observation is in accordance with other wake measurements [44] [45] and CFD simulations [4]. At this point, a comparison between the measured wakes at $x/D = 9$ from test case A using T3 and test case B using T1 is made. The result is given in Figure 10. A blockage effect elimination is applied to achieve approximately the same inflow velocity. Both rotors utilize the same airfoil. Furthermore, the wake velocity as well as downstream and horizontal distances are normalized. Consequently, an identical or at least a very similar result is expected. Conversely, the percentage difference in centerline velocity and available power extractable for a downstream turbine amounts 7.1 % and 19.3 %, respectively. This is most likely primarily caused by the different power coefficients of both turbines at operating tip speed ratio. Due to the downscaling, the design of turbine T3 is not optimized and low Reynolds number of about 60 000 are reached. Whereas, the S826 airfoil performs best above 70 000 to 100 000 [46]. Consequently, the turbine is characterized by a lower power coefficient. The corresponding power and thrust curves are given in Figure B.1. Since power coefficient are $C_{P,T1} \approx 0.46$ and $C_{P,T3} \approx 0.33$, turbine T3 extracts roughly 30 % less power from the wind. Furthermore, the mismatch could be caused by the difference in ambient turbulence intensity at $x/D = 9$. Due to the different rotor size, $x/D_{T1} = 9$ is signifi-

Table 5: Test case B: Wake prediction results using the comparison methods MAPE and APPE at blade pitch angles $\beta = 0°, \beta = 2°, \beta = 5°$ and downstream distances $x/D = 3, 5, 9$

		$\beta = 0°$		$\beta = 2°$		$\beta = 5°$	
		MAPE [%]	APPE [%]	MAPE [%]	APPE [%]	MAPE [%]	APPE [%]
$x/D = 3$	Jensen	6.8	12.6	6.3	5.5	5.4	5.4
	Larsen	16.4	−93.0	9.1	−28.9	6.3	2.5
	Frandsen	19.6	−105.4	13.2	−51.6	8.6	−22.7
	Ishihara	10.9	12.3	10.5	25.1	10.1	31.4
	BP	9.0	1.9	9.0	20.9	8.1	21.6
	JGWM	10.5	−2.2	9.4	4.5	7.7	9.5
$x/D = 5$	Jensen	7.3	−8.4	6.7	−11.1	6.1	−9.6
	Larsen	14.9	−85.8	8.8	−36.2	5.4	−9.7
	Frandsen	17.9	−97.3	13.1	−58.1	9.9	−34.2
	Ishihara	4.5	−13.3	5.2	4.2	5.9	14.1
	BP	7.7	−31.8	5.1	−10.2	5.1	−2.8
	JGWM	4.8	−14.6	5.1	−6.1	5.1	−1.4
$x/D = 9$	Jensen	7.6	−21.7	7.0	−20.3	6.1	−14.5
	Larsen	10.1	−59.1	6.7	−29.1	4.5	−8.9
	Frandsen	12.2	−69.5	9.9	−47.2	7.7	−29.0
	Ishihara	5.3	−24.5	3.4	−7.7	3.6	5.2
	BP	8.1	−43.5	6.3	−26.6	5.2	−14.8
	JGWM	4.3	−19.4	3.5	−11.4	3.0	−4.8

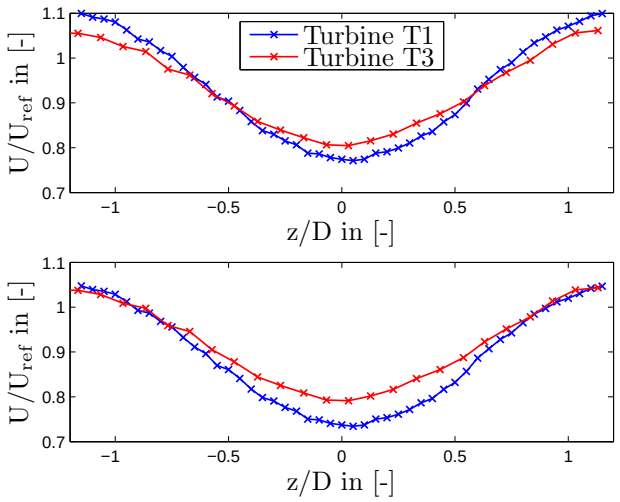

Figure 10: Measured line wake comparison at $x/D = 9$ and $I_a = 10\,\%$ between turbine T1 and T3 **(top:)** without and **(bottom:)** with blockage effect correction

cantly further downstream than $x/D_{T3} = 9$. Hence, due to the turbulence decay in the wind tunnel, the ambient turbulence intensity amounts approximately $I_{a,9D,T1} = 2.9\,\%$ and $I_{a,9D,T3} = 4.3\,\%$. Since wake recovery is a function of ambient turbulence intensity, the wake recovery is slightly higher using turbine T3.

As mentioned before, the wake models are unable to predict the double-Gaussian wake shape in the near wake. Therefore, the models are evaluated using mainly the available power comparison method APPE, which is given in Table 5.

The **Jensen model** shows high sensitivity to a change of blade pitch angle. Therefore, regarding a certain downstream distance and varying the pitch angle yields a very similar APPE at all angles. Particularly, at $x/D = 3$ and $x/D = 5$ the available power in the wake is reasonable predicted. Conversely, as expected, the model strongly overestimates the wake velocity at $x/D = 9$ and thus the available power at all pitch angles. The absolute average APPE at all nine cases amounts 12.1 %

The **Larsen model** is characterized by a decrease of wake velocity with increasing blade pitch angle. This observation is contradictory to theory and measurements. Therefore, the Larsen model can not be recommended for application in wind farm control optimization.

Same applies to the **Frandsen model**, which again strongly overestimates the wake velocity and thus available power. Furthermore, the model almost shows no sensitivity to a change of rotor thrust at all.

The **Ishihara model** also reacts insufficiently to blade pitch angle variation. Pitching the blade from $\beta = 0°$ to 5° results in a centerline velocity percentage change of only 0.9 %. However, the predicted wake is always roughly in magnitude of the measurements. Therefore, the absolute average APPE amounts 15.3 %, which is a reasonable result regarding the above mentioned increased near wake length and ambient turbulence intensity decay.

The same insensitivity according to a change of blade pitch angle applies to the **BP model**. Further-

Table 6: Test case C: Upstream turbine power and thrust coefficient measurement and modelling comparison at operating and design tip speed ratio $\lambda_{up} = 6$

		$\beta = 0°$	$\beta = 2°$	$\beta = 5°$
C_P	Experiment	0.467	0.413	0.289
	BEM w/ BC	0.468	0.430	0.329
	BEM w/o BC	0.404	0.383	0.302
C_T	Experiment	0.828	0.695	0.517
	BEM w/ BC	0.848	0.717	0.504
	BEM w/o BC	0.792	0.675	0.478

more, a similar wake recovery with downstream distances can be observed between the two models. However, the BP model predicts a higher wake velocity in magnitude of roughly 10 % than the Ishihara model at all nine cases. Therefore, the model also overestimates the measured wake velocity, in particular in the far wake. Accordingly, the average APPE amounts 19.3 %.

The **adjusted Jensen-Gaussian wake model** reacts more sensitive to blade pitch angle variation than the other wake models, except the Jensen model. However, the caused wake velocity reduction through pitch angle variation is still slightly underestimated. Nevertheless, the model shows good agreement with the measurement, particularly at $x/D = 3$ and $x/D = 5$. An absolute average APPE of only 8.2 % represents the best wake flow prediction. Consequently, the adjusted Jensen-Gaussian wake model shows the best prediction performance at both test cases.

3.2 Performance prediction

In this section, performance measurements of upstream and downstream turbine are compared to BEM method calculations. Upstream turbine power and thrust measurements and calculations at three different pitch angles $\beta = 0°$, 2° and 5° are applied. Hence, the BEM method's suitability for wind farm pitch control applications can be assessed. To take wind tunnel blockage effects into account, a blockage effect correction is applied to the modelled thrust and power coefficients. In order to model the downstream turbine performance, the adjusted Jensen-Gaussian wake model is used. Additionally, two velocity calculation methods are compared, the mean-blade-element-velocity and the mean-rotor-velocity method. Finally, the measured and predicted combined power output of upstream and downstream turbine are compared and evaluated.

3.2.1 Upstream Turbine

Upstream power and thrust measurement and modelling results are given in Figure 11. To emphasise the strong influence of blockage on the turbine's performance, the corrected as well as non-corrected thrust and power coefficients are displayed. The resulting power and thrust coefficients at design tip speed ratio $\lambda_D = 6$ are displayed in Table 6.

At $\beta = 0°$ the measured power coefficient is almost perfectly predicted by the BEM method, in particular up to $\lambda = 8$. At design TSR the prediction error amounts only 0.2 %. From $\lambda = 8$ the BEM method slightly overestimates the measured power coefficient. Same applies to the runaway point, at which the power coefficient equals zero. The thrust coefficient is very well predicted in the range between $\lambda = 4$ and $\lambda = 8$. At design TSR the prediction error only amounts 2.4 %. Up to $\lambda = 4$ the BEM method underestimates the measured thrust, whereas it is slightly overestimated from $\lambda = 8$.

As described earlier, pitching the rotor blades results in a reduction of the angle of attack and therefore a lift reduction and drag increase. Consequently, the power output and thrust decreases. Hence, at $\beta = 2°$ the measured power at design TSR decreases by 11.6 % and thrust by 16.1 %. However, the BEM method slightly overestimates the power from about $\lambda = 4$ to the runaway point. Therefore, the prediction error increases to 4.1 %. Furthermore, a shift of maximum power point and runaway point towards smaller tip speed ratios can be observed. The TSR at maximum power point amounts $\lambda = 5.37$. Both effects are predicted by the simulation, however, power coefficient at $\lambda = 5.37$ and the runaway TSR are slightly overestimated. Accordingly, at $\lambda = 5.37$ the measured power coefficient amounts $C_{P,meas} = 0.421$, whereas the modelled coefficient is $C_{P,BEM,BC} = 0.436$. This represents a prediction error of 3.6 %. The thrust coefficient is very accurately predicted in the range between $\lambda = 3.5$ and $\lambda = 7$. At design TSR $\lambda_D = 6$ the prediction error only amounts 3.2 %. Similar to the power coefficient, from $\lambda = 7$ the BEM method overestimates the measured thrust coefficient.

Increasing the pitch angle to $\beta = 5°$ results in a further decrease of the power coefficient. Additionally, a further shift of maximum power and runaway point towards lower TSR can be observed. Thus, the maximum power point is reached at $\lambda = 4.5$, where $C_{P,meas} = 0.334$ and $C_{P,BEM,BC} = 0.362$. This represents a prediction error of 8.4 %. Furthermore, operating the turbine at $\lambda = 4.5$ yields an measured increase of the power coefficient of 23.5 % compared to an operation at design TSR. This underlines the importance of wind turbine control. The prediction error at design TSR $\lambda_D = 6$ amounts 13.8 %. Moreover, the thrust coefficient is again very accurately predicted in the range between $\lambda = 3$ and $\lambda = 7$. Therefore, the prediction error amounts 2.5 % at $\lambda_D = 6$.

In total, the BEM method including blockage effect correction shows a very high prediction accuracy of power and thrust at non-pitched blades. The accuracy of power prediction decreases with increasing pitch angle due to an overestimation of the BEM method.

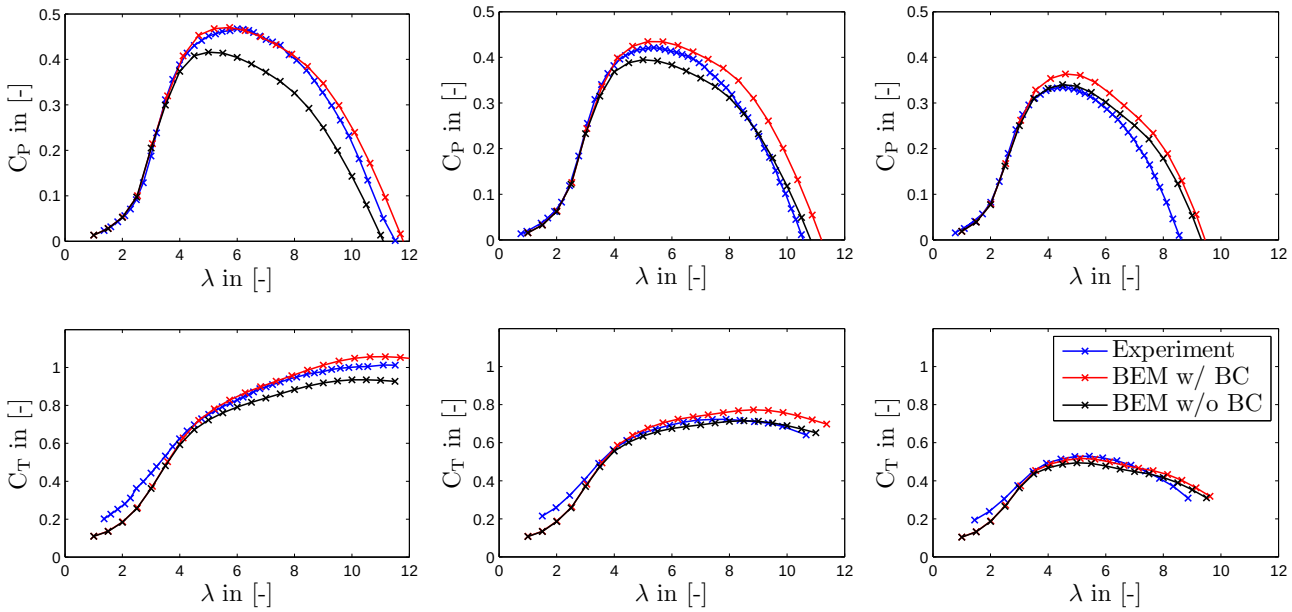

Figure 11: Test case C: Upstream turbine power and thrust measurement and modelling comparison with and without blockage effect correction at blade pitch angles **(left:)** $\beta = 0°$, **(center:)** $\beta = 2°$, **(right:)** $\beta = 5°$

However, it is still in good agreement with the measurement. Moreover, the prediction of thrust shows very high accuracy, independent on the blade pitch angle. Eventually, it should be noted that the non-blockage-corrected BEM method shows even better prediction results for power coefficient at blade pitch angles $\beta \geq 4°$. This is due to the overestimation of the BEM method at higher pitch angles.

3.2.2 Downstream Turbine

In order to model the downstream turbine performance, the following modelling scheme is used. At first, the upstream turbine thrust coefficient is calculated using the BEM equations. Subsequently, a blockage effect correction is applied. The corrected thrust coefficient, in turn, is used as input parameter to the adjusted Jensen-Gaussian wake model. Subsequently, the wake model predicts the wake velocity depending on the downstream turbine position. Furthermore, two velocity calculation methods, mean-blade-element-velocity (MBEV) and mean-rotor-velocity (MRV) are used to compute the inflow velocity to the BEM equations. Finally, the downstream turbine power and thrust can be calculated and blockage effect corrected. In total, power measurements at three downstream distances $x/D = 3, 5$ and 9 and three upstream turbine pitch angles $\beta = 0°, 2°$, and 5° are conducted. The resulting measured and modelled power coefficients are displayed in Figure 12. Power coefficients at operating tip speed ratio $\lambda = 4.5$ are given in Table 7. Thrust measurements are also conducted at $x/D = 3, 5$ and 9, however, only at $\beta = 0°$. Resulting measured and modelled thrust coefficient are displayed in Figure B.9.

As expected, pitching the upstream turbine blades results in an increase of downstream turbine power. Moreover, due to wake recovery, the power further increases with increasing downstream distances. Either simulation methods are able to model these trends. At $x/D = 3$ the MBEV method overestimated the measured power coefficient at all pitch angles. Conversely, the MRV method underestimates the power output. Similar applies at $x/D = 5$, at which the MBEV method still overestimates the measured power coefficient. Whereas the MRV method predicts the measurement very accurately with only a slight underestimation. At $x/D = 9$ both methods show a very high prediction accuracy, in particular the MBEV method. Consequently, the prediction error at operating TSR only amounts 2.9 % on average at $x/D = 9$. The absolute average prediction error at all downstream distances and blade pitch angles amounts 9.3 % for the MBEV method and 7.3 % for the MRV method. Contrarily, the thrust coefficient comparison yields a significantly better prediction using the MBEV method at all downstream distances. However, in order to finally assess the downstream power prediction accuracy, the wake and performance prediction have to be separated. Therefore, potential neutralization effects can be avoided. The wake comparison from section 3.1.2 yields an overestimation of the available power in the wind at downstream distances $x/D = 5$ and 9. Consequently, one would assume an overestimation of the downstream power. Contrarily, the MRV method underestimates the power coefficient at all downstream distances and all pitch angles, except $x/D = 9$ and $\beta = 5°$. In order to verify this assumption, the downstream turbine power is computed using a measured fullwake as input to the BEM equations. As expected, the result, given in Figure B.2, reveals a significant underestimation of the power coefficient using the MRV

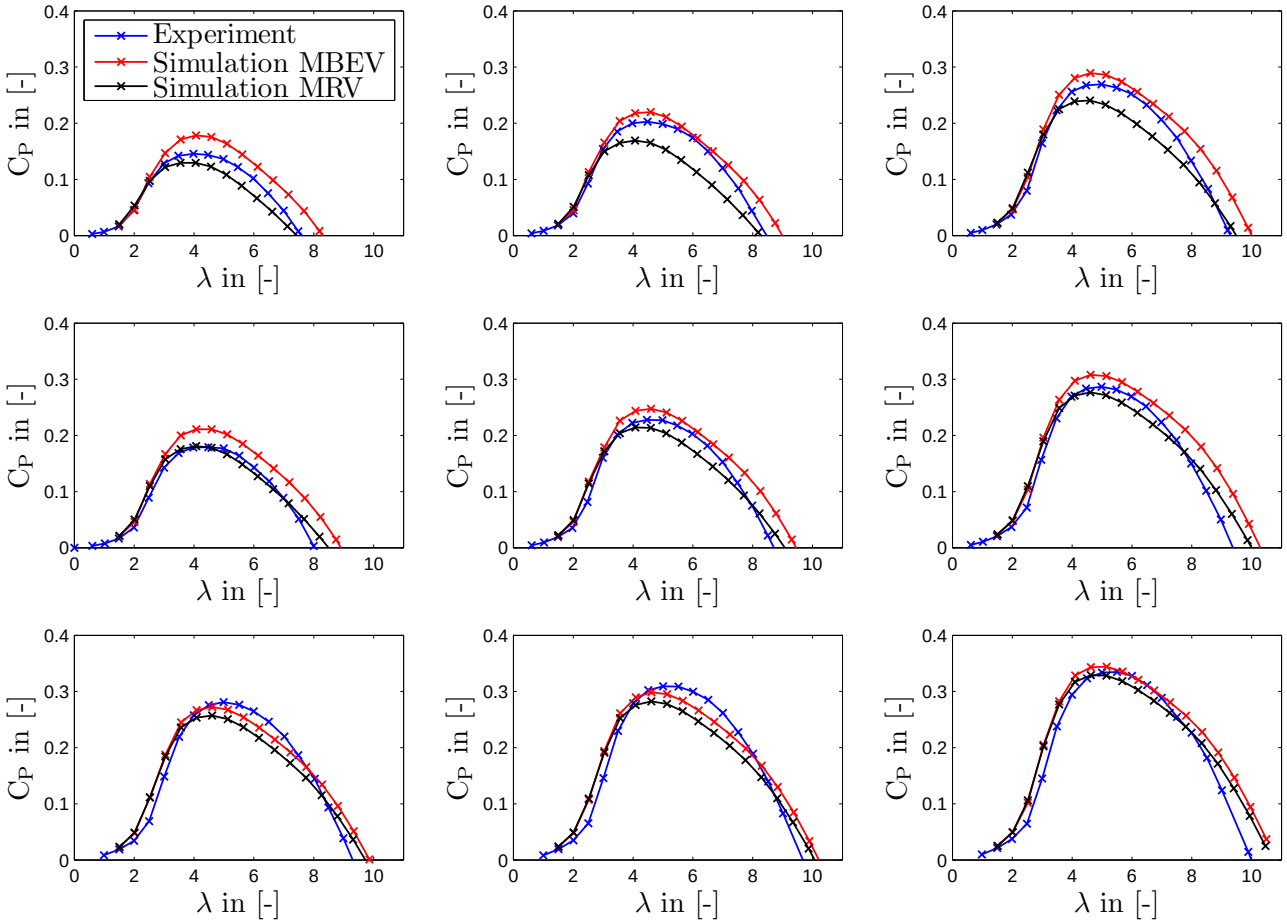

Figure 12: Test case C: Downstream turbine power measurement and modelling comparison using the mean-blade-element-velocity (MBEV) and mean-rotor-velocity (MRV) methods at blade pitch angles **(left row:)** $\beta = 0°$, **(center row:)** $\beta = 2°$, **(right row:)** $\beta = 5°$ and downstream distances **(top column:)** $x/D = 3$, **(center column:)** $x/D = 5$, **(bottom column:)** $x/D = 9$

method. Consequently, the MRV method yields a less accurate result considering exclusively the downstream performance prediction. However, taking the overall simulation process into account, the method gives the better power prediction.

In general, the downstream turbine performance predictions are performing fairly well considering the complex wake flow they are exposed to. However, a lower prediction accuracy can be observed modelling the downstream turbine power compared to the upstream turbine power. This is caused by the additional wake prediction, which contains an additional prediction uncertainty. An increase of downstream turbine performance prediction inaccuracy can be also observed in several CFD simulations [28].

3.2.3 Combined power output

The resulting combined power output of upstream and downstream turbine at operating tip speed ratios is given in Table 8. Evidentially, applying blade pitch control does not result in an increase of combined power output. Only at downstream turbine position $x/D = 3$ and upstream turbine pitch angle $\beta = 2°$ a very slight increase of 1 % can be measured. The simulations also only yield an increase at $x/D = 3$ and $\beta = 2°$ of up to 1 %. However, beside only optimizing a wind farm power output, mechanical loads have to be considered as well. Pitching the upstream turbine results in a decrease of turbulence intensity in the wake. Consequently, a downstream turbine located in the wake experiences less turbulence intensity. The modelled turbulence intensities at all blade pitch angles using the Crespo and Hernandez model are displayed in Figure B.10. As an example, increasing the pitch angle from $\beta = 0°$ to $\beta = 2°$ results in a power decrease of less than 1 % at $x/D = 5$. This value is almost negligible. However, the decrease of turbulence intensity amounts 16.7 %. As mentioned earlier turbulence intensity influences the turbine lifespan, which, in turn, affects the profitability. Therefore, small upstream turbine pitch angles could be an interesting option, when optimizing wind farm control.

In total, the MBEV method overestimates the combined power output at every downstream distance and pitch angle. However, in particular in the far wake and at small pitch angles, the method performs well. The average prediction error amounts 6.2 %. Apply-

Table 7: Test case C: Downstream turbine power coefficient measurement and modelling comparison at operating tip speed ratio $\lambda_{\text{down}} = 4.5$

	$x/D = 3$			$x/D = 5$			$x/D = 9$		
	$\beta = 0°$	$\beta = 2°$	$\beta = 5°$	$\beta = 0°$	$\beta = 2°$	$\beta = 5°$	$\beta = 0°$	$\beta = 2°$	$\beta = 5°$
Experiment	0.143	0.203	0.268	0.179	0.228	0.284	0.276	0.302	0.323
Simulation MBEV	0.177	0.220	0.289	0.212	0.247	0.307	0.272	0.298	0.342
Simualtion MRV	0.124	0.166	0.241	0.179	0.214	0.276	0.257	0.282	0.328

Table 8: Test case C: Combined power coefficient measurement and modelling comparison at operating tip speed ratios $\lambda_{\text{up}} = 6$ and $\lambda_{\text{down}} = 4.5$

	$x/D = 3$			$x/D = 5$			$x/D = 9$		
	$\beta = 0°$	$\beta = 2°$	$\beta = 5°$	$\beta = 0°$	$\beta = 2°$	$\beta = 5°$	$\beta = 0°$	$\beta = 2°$	$\beta = 5°$
Experiment	0.610	0.616	0.557	0.646	0.641	0.573	0.743	0.715	0.612
Simulation MBEV	0.645	0.650	0.618	0.680	0.677	0.636	0.740	0.728	0.671
Simualtion MRV	0.592	0.596	0.570	0.647	0.644	0.605	0.725	0.712	0.657

ing the MRV methods yields a very high accuracy at all downstream distances and pitch angles. Therefore, the average prediction error only amounts 2.8 %.

4 Conclusions and future work

Six analytical wind turbine wake models were compared to wind tunnel measurements. Thereby, a variation of ambient turbulence intensity and blade pitch angle was conducted.

Two wake models, the Larsen and Frandsen model were found to be unable to predict the wake velocities reasonably at all test cases. The Bastankah & Porté-Agel model yielded a better wake prediction. However, due to an overestimation of the wake velocity still high prediction errors were reached. The Ishihara model was found to predict the measured wake velocity very accurately at high ambient turbulence intensity and non-pitched blades. However, the model shows a high insensitivity towards a change of blade pitch angle. Conversely, the Jensen model revealed a high and sufficient sensitivity to pitch variation. Furthermore, it gave an accurate prediction at high ambient turbulence intensity. Solely, at low ambient turbulence intensity the model was unable to predict the wake velocity at all. Nevertheless, the model was assessed to be suitable for application in wind farm wake modelling. The original Jensen-Gaussian wake model used a turbulence intensity model, which was found to be unable to accurately predict the wake velocity at low ambient turbulence intensities. Consequently, the adjustment to combine the wake model with another turbulence intensity model was proposed in this work. The combination with the Crespo and Hernandez turbulence model showed a significant improvement at all test cases. Eventually, the model was found to give the best overall performance.

A Blade Element Momentum method with guaranteed convergence was applied to model upstream and downstream turbine performances. Furthermore, the adjusted Jensen-Gaussian wake model and a two velocity-calculation methods were used to predict the downstream turbine power and thrust. All modelling results were compared to wind tunnel measurements.

The upstream power as well as thrust coefficient were very accurately predicted, in particular at non-pitched blades. A slight deviation was found at pitch angles greater than two degrees. The downstream turbine performance was found to be fairly well predicted using the mean-rotor-velocity method. Consequently, the averaged combined power output prediction error at all downstream and pitch angles amounted only 2.8 %. Using the mean-blade-element-velocity method resulted in a slightly higher prediction error, even though it takes the non-uniform inflow into account. This was due to a constant overestimation of the power coefficient. Therefore, the overall prediction error was 6.2 %. In summary, the adjusted Jensen-Gaussian wake model and the mean-rotor-velocity method are recommended for application in wind farm modelling.

In order to apply those methods to a wind farm, which consists of more than four wind turbines, multiple wake superposition has to be investigated. Several models are available for this purpose, however, no validation with wind tunnel measurements are known yet. Therefore, a validation of multiple wake models with wind tunnel measurements could be the aim of future research. Moreover, investigations of an offset downstream turbine could be useful in order to further consider partial wake interactions. A simulation could be easily done using the above mentioned simulation method. However, the biggest challenge would be to take the increased blockage effect into account. Due to the offset downstream turbine a higher blockage ratio occurs in the wind tunnel. Similar measurements were already conducted by Krogstad et al. [47], however,

only at a separation distance of three rotor diameters. A higher separation distance should be applied to reduce the blockage effect and consider realistic wind farm turbine spacings. Furthermore, as mentioned in section 3.1.1, the effect of turbulence intensity on wake expansion could be investigated further. For this purpose a constant ambient turbulence intensity has to be installed in the wind tunnel. This could be done by mounting inclinable boards in periodic spacings on the wind tunnel floor. An alternative and probably more effortless approach are CFD simulations with constant ambient turbulence intensity.

References

[1] S Andrew Ning. A simple solution method for the blade element momentum equations with guaranteed convergence. *Wind Energy*, 17(9):1327–1345, 2014.

[2] Jaeha Ryi, Wook Rhee, Ui Chang Hwang, and Jong-Soo Choi. Blockage effect correction for a scaled wind turbine rotor by using wind tunnel test data. *Renewable Energy*, 79:227–235, 2015.

[3] LJ Vermeer, Jens Nørkær Sørensen, and A Crespo. Wind turbine wake aerodynamics. *Progress in aerospace sciences*, 39(6):467–510, 2003.

[4] Jens N Sørensen, Robert Mikkelsen, Sasan Sarmast, Stefan Ivanell, and Dan Henningson. Determination of wind turbine near-wake length based on stability analysis. In *Journal of Physics: Conference Series*, volume 524, page 012155. IOP Publishing, 2014.

[5] Rebecca Jane Barthelmie, K Hansen, Sten Tronæs Frandsen, Ole Rathmann, JG Schepers, W Schlez, J Phillips, K Rados, A Zervos, ES Politis, et al. Modelling and measuring flow and wind turbine wakes in large wind farms offshore. *Wind Energy*, 12(5):431–444, 2009.

[6] Rebecca Jane Barthelmie, SC Pryor, Sten Tronæs Frandsen, Kurt Schaldemose Hansen, JG Schepers, K Rados, W Schlez, A Neubert, LE Jensen, and S Neckelmann. Quantifying the impact of wind turbine wakes on power output at offshore wind farms. *Journal of Atmospheric and Oceanic Technology*, 27(8):1302–1317, 2010.

[7] Amin Niayifar and Fernando Porté-Agel. Analytical modeling of wind farms: A new approach for power prediction. *Energies*, 9(9):741, 2016.

[8] M Gaumond, Pierre-Elouan Réthoré, Andreas Bechmann, Søren Ott, Gunner Chr Larsen, Alfredo Pena Diaz, and KS Kurt. Benchmarking of wind turbine wake models in large offshore windfarms. *Proceedings of the Science of Making Torque From Wind*, 2012.

[9] RJ Barthelmie, GC Larsen, ST Frandsen, L Folkerts, K Rados, SC Pryor, B Lange, and G Schepers. Comparison of wake model simulations with offshore wind turbine wake profiles measured by sodar. *Journal of atmospheric and oceanic technology*, 23(7):888–901, 2006.

[10] Jason R Marden, Shalom D Ruben, and Lucy Y Pao. A model-free approach to wind farm control using game theoretic methods. *IEEE Transactions on Control Systems Technology*, 21(4):1207–1214, 2013.

[11] Tomislav Horvat, Vedrana Spudić, and Mato Baotić. Quasi-stationary optimal control for wind farm with closely spaced turbines. In *MIPRO, 2012 Proceedings of the 35th International Convention*, pages 829–834. IEEE, 2012.

[12] Jaejoon Lee, Eunkuk Son, Byungho Hwang, and Soogab Lee. Blade pitch angle control for aerody-

namic performance optimization of a wind farm. *Renewable energy*, 54:124–130, 2013.

[13] Niels Otto Jensen. *A note on wind generator interaction*. 1983.

[14] I Katic, J Højstrup, and Niels Otto Jensen. A simple model for cluster efficiency. pages 407–410, 1986.

[15] Gunner Chr Larsen. *A simple wake calculation procedure*. 1988.

[16] Gunner Chr Larsen. A simple stationary semi-analytical wake model. Technical report, Risø National Laboratory for Sustainable Energy, Technical University of Denmark, 2009.

[17] Takeshi Ishihara, Atsushi Yamaguchi, and Yozo Fujino. Development of a new wake model based on a wind tunnel experiment. Technical report, Global Wind, Technical Report, http://windeng. tu-tokyo. ac. jp/ishihara/-posters/2004_gwp_poster. pdf, 2004.

[18] Sten Frandsen, Rebecca Barthelmie, Sara Pryor, Ole Rathmann, Søren Larsen, Jørgen Højstrup, and Morten Thøgersen. Analytical modelling of wind speed deficit in large offshore wind farms. *Wind energy*, 9(1-2):39–53, 2006.

[19] Majid Bastankhah and Fernando Porté-Agel. A new analytical model for wind-turbine wakes. *Renewable Energy*, 70:116–123, 2014.

[20] Xiaoxia Gao, Hongxing Yang, and Lin Lu. Optimization of wind turbine layout position in a wind farm using a newly-developed two-dimensional wake model. *Applied Energy*, 174:192–200, 2016.

[21] Martin Otto Laver Hansen. Aerodynamics of wind turbines. 2008.

[22] Ian Masters, JC Chapman, MR Willis, and JAC Orme. A robust blade element momentum theory model for tidal stream turbines including tip and hub loss corrections. *Journal of Marine Engineering & Technology*, 10(1):25–35, 2011.

[23] Michael McWilliam and Curran Crawford. The behavior of fixed point iteration and newton-raphson methods in solving the blade element momentum equations. *Wind Engineering*, 35(1):17–31, 2011.

[24] P-Å Krogstad and JA Lund. An experimental and numerical study of the performance of a model turbine. *Wind Energy*, 15(3):443–457, 2012.

[25] Luis Garcıa, Mari Vatn, Franz Mühle, and Lars Sætran. Experiments in the wind turbine far wake for the evaluation of an analytical wake model.

[26] Dan M Somers. The s825 and s826 airfoils. *National Renewable Energy Laboratory, Subcontractor Report*, 2005.

[27] ML Thørgersen, T Sørensen, Per Nielsen, A Grötzner, and Stefan Chun. Windpro/park: introduction to wind turbine wake modelling and wake generated turbulence. *EMD International A/S, Aalborg, Denmark*, 2005.

[28] Jan Bartl and Lars Sætran. Blind test comparison of the performance and wake flow between two in-line wind turbines exposed to different turbulent inflow conditions. *Wind Energy Science*, 2(1):55–76, 2017.

[29] Rob J Hyndman and Anne B Koehler. Another look at measures of forecast accuracy. *International journal of forecasting*, 22(4):679–688, 2006.

[30] TY Chen and LR Liou. Blockage corrections in wind tunnel tests of small horizontal-axis wind turbines. *Experimental Thermal and Fluid Science*, 35(3):565–569, 2011.

[31] Alfredo Peña, Pierre-Elouan Réthoré, and M Paul Laan. On the application of the jensen wake model using a turbulence-dependent wake decay coefficient: the sexbierum case. *Wind Energy*, 2015.

[32] Per Nielsen. Windpro 2.7 user guide 3. edition. *EMD International A/S*, 2010.

[33] Linlin Tian, Weijun Zhu, Wenzhong Shen, Ning Zhao, and Zhiwei Shen. Development and validation of a new two-dimensional wake model for wind turbine wakes. *Journal of Wind Engineering and Industrial Aerodynamics*, 137:90–99, 2015.

[34] Sten Tronæs Frandsen, L Chacón, A Crespo, P Enevoldsen, R Gómez-Elvira, J Hernández, J Højstrup, F Manuel, and K Thomsen. Measurements on and modelling of offshore wind farms. Technical report, 1996.

[35] A Crespo, J Herna, et al. Turbulence characteristics in wind-turbine wakes. *Journal of wind engineering and industrial aerodynamics*, 61(1):71–85, 1996.

[36] Unsal Hassan. *A wind tunnel investigation of the wake structure within small wind turbine farms*. Harwell Laboratory, Energy Technology Support Unit, 1993.

[37] DC Quarton and JF Ainslie. Turbulence in wind turbine wakes. *Wind Engineering*, pages 15–23, 1990.

[38] Richard P. Brent. An algorithm with guaranteed convergence for finding a zero of a function. *The Computer Journal*, 14(4):422–425, 1971.

[39] Patrick J Moriarty and A Craig Hansen. Aerodyn theory manual. Technical report, National Renewable Energy Lab., Golden, CO (US), 2005.

[40] Marshall L Buhl Jr. New empirical relationship between thrust coefficient and induction factor for the turbulent windmill state. Technical report, National Renewable Energy Laboratory (NREL), Golden, CO., 2005.

[41] Bernhard Lange, Hans-Peter Waldl, Algert Gil Guerrero, Detlev Heinemann, and Rebecca J Barthelmie. Modelling of offshore wind turbine wakes with the wind farm program flap. *Wind Energy*, 6(1):87–104, 2003.

[42] Heiner Schümann, Fabio Pierella, and Lars Sætran. Experimental investigation of wind turbine wakes in the wind tunnel. *Energy Procedia*, 35:285–296, 2013.

[43] Robert W Baker and Stel N Walker. Wake mea-

surements behind a large horizontal axis wind turbine generator. *Solar Energy*, 33(1):5–12, 1984.

[44] Clio Ceccotti, Andrea Spiga, Jan Bartl, and Lars Sætran. Effect of upstream turbine tip speed variations on downstream turbine performance. *Energy Procedia*, 94:478–486, 2016.

[45] J Bartl and L Sætran. Experimental testing of axial induction based control strategies for wake control and wind farm optimization. In *Journal of Physics: Conference Series*, volume 753, page 032035. IOP Publishing, 2016.

[46] H Sarlak, R Mikkelsen, Sasan Sarmast, and Jens Nørkær Sørensen. Aerodynamic behaviour of nrel s826 airfoil at re= 100,000. In *Journal of Physics: Conference Series*, volume 524, page 012027. IOP Publishing, 2014.

[47] Per-Åge Krogstad, Lars Sætran, and Muyiwa Samuel Adaramola. "blind test 3" calculations of the performance and wake development behind two in-line and offset model wind turbines. *Journal of Fluids and Structures*, 52:65–80, 2015.

[48] Jens N Sorensen, Wen Zhong Shen, and Robert Mikkelsen. Wall correction model for wind tunnels with open test section. *AIAA journal*, 44(8):1890–1894, 2006.

[49] PEJ Vermeulen. An experimental analysis of wind turbine wakes. In *3rd international symposium on wind energy systems*, pages 431–450, 1980.

A Appendix: Derivations

A.1 Blockage effect correction

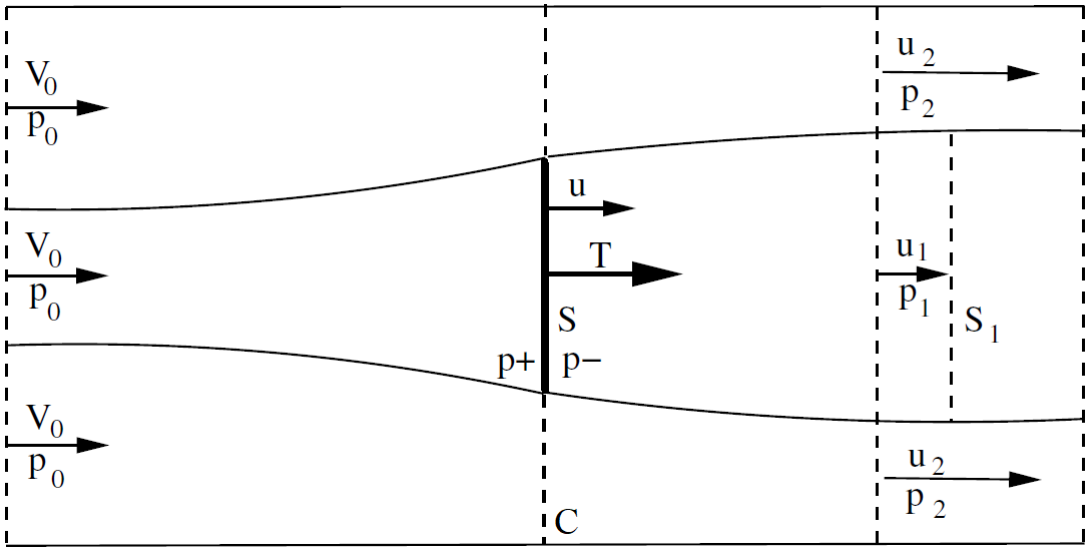

Figure A.1: Rotor disk in closed wind tunnel, adapted from [48]

Figure A.1 shows a uniform airstream with inflow velocity V_0 passing through an actuator disk with cross section S located in a wind tunnel with cross section area C. The flow is assumed to be incompressible, inviscid and axisymmteric [48]. The continuity equation inside of the slipstream and between the slipstream and the tunnel walls gives

$$u_1 S_1 = uS \tag{A.1}$$

$$u_2(C - S_1) = V_0 C - uS \tag{A.2}$$

Applying the Bernoulli equation outside the slipstream gives

$$p_0 + \frac{1}{2}\rho V_0^2 = p_1 + \frac{1}{2}\rho u_2^2 \tag{A.3}$$

$$p_1 - p_0 = \frac{1}{2}\rho(V_0^2 - u_2^2) \tag{A.4}$$

Inside of the slipstream the pressure jump across the disc is directly proportional to the thrust, hence

$$T/S = p'_+ - p'_- \tag{A.5}$$

Applying the Bernoulli equation inside of the slipstream and using Eqs. (A.4) and (A.5) gives

$$p_0 + \frac{1}{2}\rho V_0^2 + p'_+ = p_1 + \frac{1}{2}\rho u_1^2 + p'_- \tag{A.6}$$

$$p'_+ - p'_- = p_1 - p_0 + \frac{1}{2}\rho(u_1^2 - V_0^2) \tag{A.7}$$

$$T = \frac{1}{2}\rho S(u_1^2 - u_2^2) \tag{A.8}$$

Applying the momentum equation on the whole tunnel gives

$$T - (p_1 - p_0)C = \rho u_1 S_1(u_1 - V_0) - \rho u_2(C - S1)(V_0 - u_2) \tag{A.9}$$

Since the thrust of an actuator disk is identical to the momentum change, the thrust in free air condition can be calculated as following

$$T = 2S\rho u(u - V') \tag{A.10}$$

Applying the following non-dimensional parameters

$$C_\mathrm{T} = \frac{2T}{\rho V_0^2 S}, \qquad C_\mathrm{P} = \frac{2(p_1 - p_0)}{\rho V_0^2}, \qquad \alpha = \frac{S}{C}, \qquad \beta = \frac{S_1}{C} \tag{A.11}$$

$$u = \frac{u}{V_0}, \qquad u_1 = \frac{u_1}{V_0}, \qquad u_2 = \frac{u_2}{V_0}, \qquad U_\mathrm{cor} = \frac{U_\mathrm{cor}}{V_0} \tag{A.12}$$

on equations (A.1), (A.2), (A.4), (A.8), (A.9) and (A.10) yields

$$\alpha u = \beta u_1 \tag{A.13}$$

$$1 = \beta u_1 + (1-\beta) u_2 \tag{A.14}$$

$$C_\mathrm{p} = 1 - u_2^2 \tag{A.15}$$

$$C_\mathrm{T} = u_1^2 - u_2^2 \tag{A.16}$$

$$C_\mathrm{T}\alpha - C_\mathrm{p} = 2\beta u_1 (u_1 - 1) - 2(1-\beta) u_2 (1 - u_2) \tag{A.17}$$

$$C_\mathrm{T} = 4u(u - U_\mathrm{cor}) \tag{A.18}$$

From the blockage ratio known and the thrust coefficient measured or simulated one can determine the remaining six unknowns. For calculating this system of non-linear equations the MATLAB function “fsolve” is used. The looked for value is the corrected normalized inflow velocity U_cor.

A.2 Larsen model

The parameters x_0 and c_1 from the Larsen model are defined as follows

$$x_0 = \frac{9.6 D_0}{\left(2R_{9.6}/kD_0\right)^3 - 1} \tag{A.19}$$

$$c_1 = \left(\frac{kD_0}{2}\right)^{5/2} \left(\frac{105}{2\pi}\right)^{-1/2} \left(C_\mathrm{T} A_0 x_0\right)^{-5/6}, \tag{A.20}$$

with the rotor area A and

$$k = \sqrt{\frac{1}{2\sqrt{1 - C_\mathrm{T}}} + \frac{1}{2}}. \tag{A.21}$$

The wake Radius $R_{9.6}$ at 9.6 rotor diameter downstream is approximated from

$$R_{9.6} = a_1 \exp\left(a_2 C_\mathrm{T}^2 + a_3 C_\mathrm{T} + a_4\right) \left(b_1 I_\mathrm{a} + 1\right) D_0, \tag{A.22}$$

where the empirically determined coefficient are

$$a_1 = 0.435449861, \tag{A.23}$$

$$a_2 = 0.797853685, \tag{A.24}$$

$$a_3 = -0.12480789, \tag{A.25}$$

$$a_4 = 0.136821858, \tag{A.26}$$

$$b_1 = 15.6298. \tag{A.27}$$

A.3 Near-wake length

In 1980, P. Vermeulen [49] found an empirical approach to model the near-wake length. Herein, the near wake is divided into two regions. The first region x_h is dependent on ambient (a), rotor added (λ) and shear-generated (m) turbulence intensity

$$x_\mathrm{h} = r_0 \left(\left(\frac{\mathrm{d}r}{\mathrm{d}x}\right)_a^2 + \left(\frac{\mathrm{d}r}{\mathrm{d}x}\right)_\lambda^2 + \left(\frac{\mathrm{d}r}{\mathrm{d}x}\right)_m^2 \right)^{0.5}, \tag{A.28}$$

where r_0 is defined as

$$r_0 = \frac{D}{2}\sqrt{\frac{m+1}{2}}, \tag{A.29}$$

with

$$m = \frac{1}{\sqrt{1 - C_\mathrm{T}}}. \tag{A.30}$$

The impact of ambient, rotor-added and shear-generated turbulence intensity are defined as follows

$$\left(\frac{\mathrm{d}r}{\mathrm{d}x}\right)_a^2 = \begin{cases} 2.5I_\mathrm{a} + 0.05 & , I_\mathrm{a} \geq 0.02 \\ 5I_\mathrm{a} & , I_\mathrm{a} < 0.02 \end{cases} \tag{A.31}$$

$$\left(\frac{\mathrm{d}r}{\mathrm{d}x}\right)_\lambda^2 = 0.012B\lambda, \tag{A.32}$$

$$\left(\frac{\mathrm{d}r}{\mathrm{d}x}\right)_m^2 = \frac{(1-m)\sqrt{1.49+m}}{9.76(1+m)}, \tag{A.33}$$

where B is the number of blades. Eventually, the near-wake length x_n can be computes from the first region length by

$$x_\mathrm{n} = \frac{\sqrt{0.212 + 0.145m}}{1 - \sqrt{0.212 + 0.145m}} \frac{1 - \sqrt{0.134 + 0124m}}{\sqrt{0.134 + 0.124}} x_\mathrm{h}. \tag{A.34}$$

Lange et al. [41] found a singularity at about $C_\mathrm{T} = 0.97$ and therefore proposed to set the thrust coefficient to 0.9 for values $C_\mathrm{T} > 0.9$.

A.4 Blade Element Momentum method by S.Ning

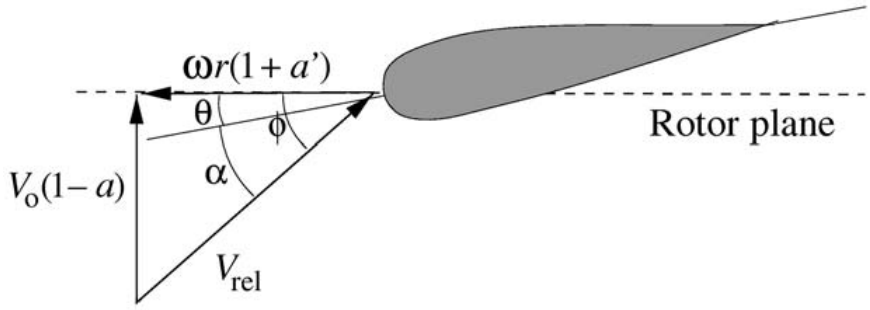

Figure A.2: Velocity components and inflow parameters at a specific blade section, from [21]

In this section, the guaranteed convergence method for the BEM equations, proposed by S. Ning [1], is presented. As explained in section 2.5 S. Ning reduced the two equation system from classical BEM theory into one equation, parametrized by the local inflow angle ϕ. The resulting algorithm to compute the local inflow at each blade element is described in detail in the following

1. Initialize the local inflow angle, for example $\phi = 45°$
2. Calculate the local angle of attack α and Reynolds number Re using the following equation

$$\alpha = \phi - (\theta + \beta), \tag{A.35}$$

where θ is the blade twist angle given by the rotor design and β the blade pitch angle. The Reynolds number is

$$Re = \frac{L_\mathrm{C} W}{\nu}, \tag{A.36}$$

where L_C is the chord length, which is given by the rotor design. W is the inflow velocity and equals V_rel from Figure A.2. It can be calculated by

$$W = \sqrt{(V_0(1-a))^2 + (\omega r(1+a'))^2}. \tag{A.37}$$

However, the induction factors are not yet known and thus the inflow velocity can not be directly computed. Therefore, an iterative solution has to be applied.

3. Read out lift C_L and drag coefficient C_D from a look-up table. They are typically given as a function of α and Re.

4. Compute normal C_n and tangential force coefficients C_t using the initialized local flow angle

$$C_\mathrm{n} = C_\mathrm{L}\cos\phi + C_\mathrm{D}\sin\phi, \tag{A.38}$$
$$C_\mathrm{t} = C_\mathrm{L}\sin\phi - C_\mathrm{D}\cos\phi. \tag{A.39}$$

5. Calculate the induction factors a and a' depending on the solution region including tip and hub loss correction. At first two non-dimensional parameters are defined

$$\kappa = \frac{\sigma C_\mathrm{n}}{4F\sin\phi^2}, \tag{A.40}$$
$$\kappa' = \frac{\sigma C_\mathrm{t}}{4F\sin\phi\cos\phi}, \tag{A.41}$$

where σ is the solidity, with number of blades B, defined as

$$\sigma = \frac{L_\mathrm{C} B}{2\pi r}. \tag{A.42}$$

Whereas, F represents the hub and tip loss correction factor. Using Prandtl's correction gives

$$f_\mathrm{tip} = \frac{B}{2}\left(\frac{R-r}{r|\sin\phi|}\right) \tag{A.43}$$
$$F_\mathrm{tip} = \frac{2}{\pi}\arccos\left(\exp\left(-f_\mathrm{tip}\right)\right) \tag{A.44}$$
$$f_\mathrm{hub} = \frac{B}{2}\left(\frac{r-R_\mathrm{hub}}{R_\mathrm{hub}|\sin\phi|}\right) \tag{A.45}$$
$$F_\mathrm{hub} = \frac{2}{\pi}\arccos\left(\exp\left(-f_\mathrm{hub}\right)\right) \tag{A.46}$$
$$F = F_\mathrm{tip}F_\mathrm{hub}. \tag{A.47}$$

Depending on the solution region, different equations must be used to compute the axial induction factors. In case of $\phi > 0$ and $\kappa \leq 2/3$ the solution is located in the momentum region

$$a = \frac{\kappa}{1+\kappa}. \tag{A.48}$$

If $\phi > 0$ and $\kappa > 2/3$, the solution falls into the empirical region

$$a = \frac{\gamma_1 - \sqrt{\gamma_2}}{\gamma_3}, \tag{A.49}$$

where

$$\gamma_1 = 2F\kappa - \left(\frac{10}{9} - F\right), \tag{A.50}$$
$$\gamma_2 = 2F\kappa - F\left(\frac{4}{3} - F\right), \tag{A.51}$$
$$\gamma_3 = 2F\kappa - \left(\frac{25}{9} - 2F\right). \tag{A.52}$$

In case of $\gamma_3 = 0$ the denominator in (A.49) becomes zero. However, same applies for the nominator. Therefore, L'Hôpital's rule can be used and yields

$$a = 1 - \frac{1}{2\sqrt{\gamma_2}}. \tag{A.53}$$

In case of a negative local inflow angle and $\kappa > 1$ the solution is located in the propeller region, where

$$a = \frac{\kappa}{\kappa - 1}. \tag{A.54}$$

If $\phi > 0$ and $\kappa \leq 1$ S. Ning proposed to set $a = 0$. Finally, the tangential induction factor, which is independent on the solution region is defined as

$$a' = \frac{\kappa'}{1 - \kappa'}. \tag{A.55}$$

6. Using a root-finding method to find the value of the local inflow angle, where the residual approaches zero. Knowing the induction factor, the residual can be calculated as follows

$$R(\phi) = \frac{\sin\phi}{1 - a} - \frac{V_0 \cos\phi}{\omega r\,(1 + a')}. \tag{A.56}$$

S. Ning proposed to use the root finding algorithm method by Brent [38] to solve the residual. The detailed solution algorithm is given in [1].

The solution of ϕ is then used to finally compute the thrust T and momentum M for each blade element

$$dT = \frac{1}{2}\rho B L_{\mathrm{C}} C_{\mathrm{n}} \frac{V_0^2 (1 - a)^2}{\sin\phi'^2} dr \tag{A.57}$$

$$dM = \frac{1}{2}\rho B L_{\mathrm{C}} C_{\mathrm{t}} \frac{V_0 (1 - a)\omega r (1 + a')}{\sin\phi' \cos\phi'} dr r \tag{A.58}$$

In order to compute the rotor thrust and power, the thrust and momentum of each blade element have to be summed up. Finally, the power is calculated by

$$P = M\omega, \tag{A.59}$$

with ω given as a function of the tip speed ratio λ

$$\omega = \frac{\lambda V_0}{R}. \tag{A.60}$$

B Appendix: Plots

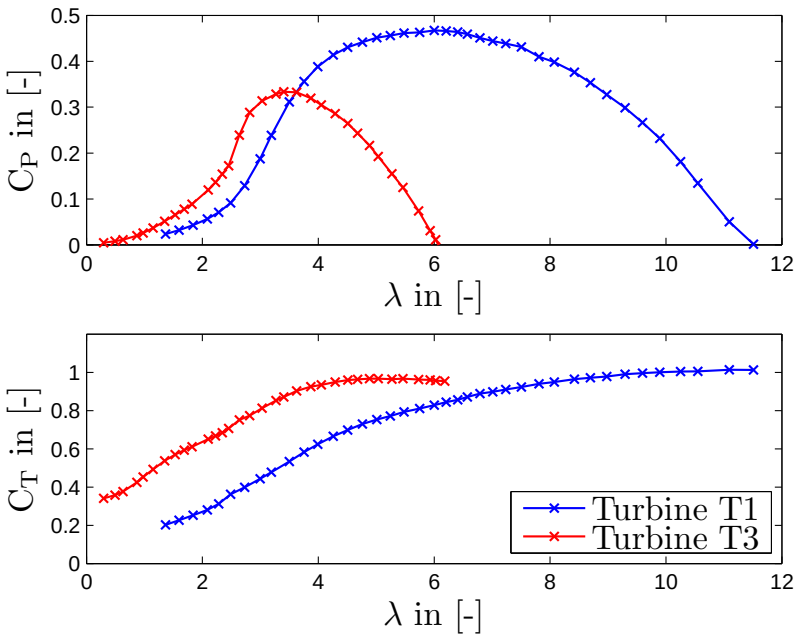

Figure B.1: Power and thrust coefficient comparison of big rotor T1 ($D = 0.944\,\mathrm{m}$) and small rotor T3 ($D = 0.450\,\mathrm{m}$)

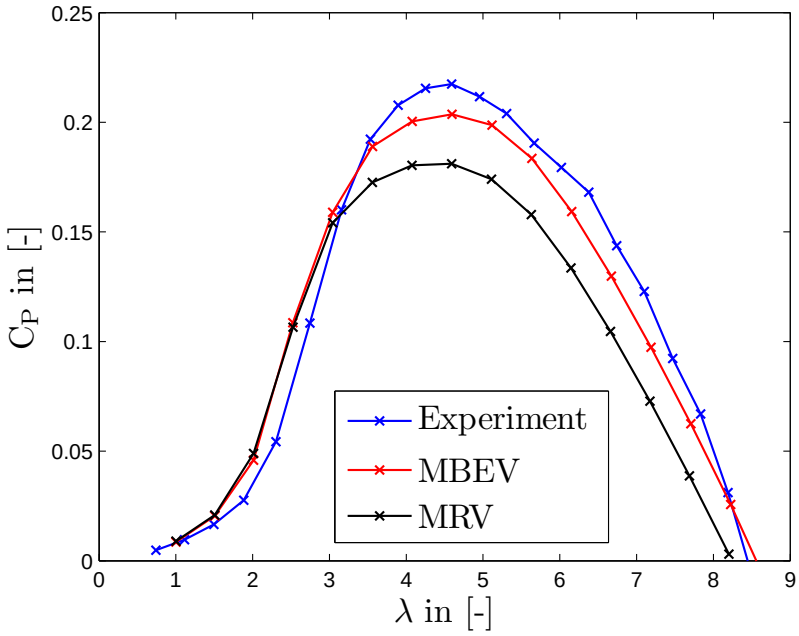

Figure B.2: Downstream turbine power coefficient measurement and modelling comparison using the measured fullwake at $x/D = 6$ and the mean-blade-element-velocity and the mean-rotor-velocity method

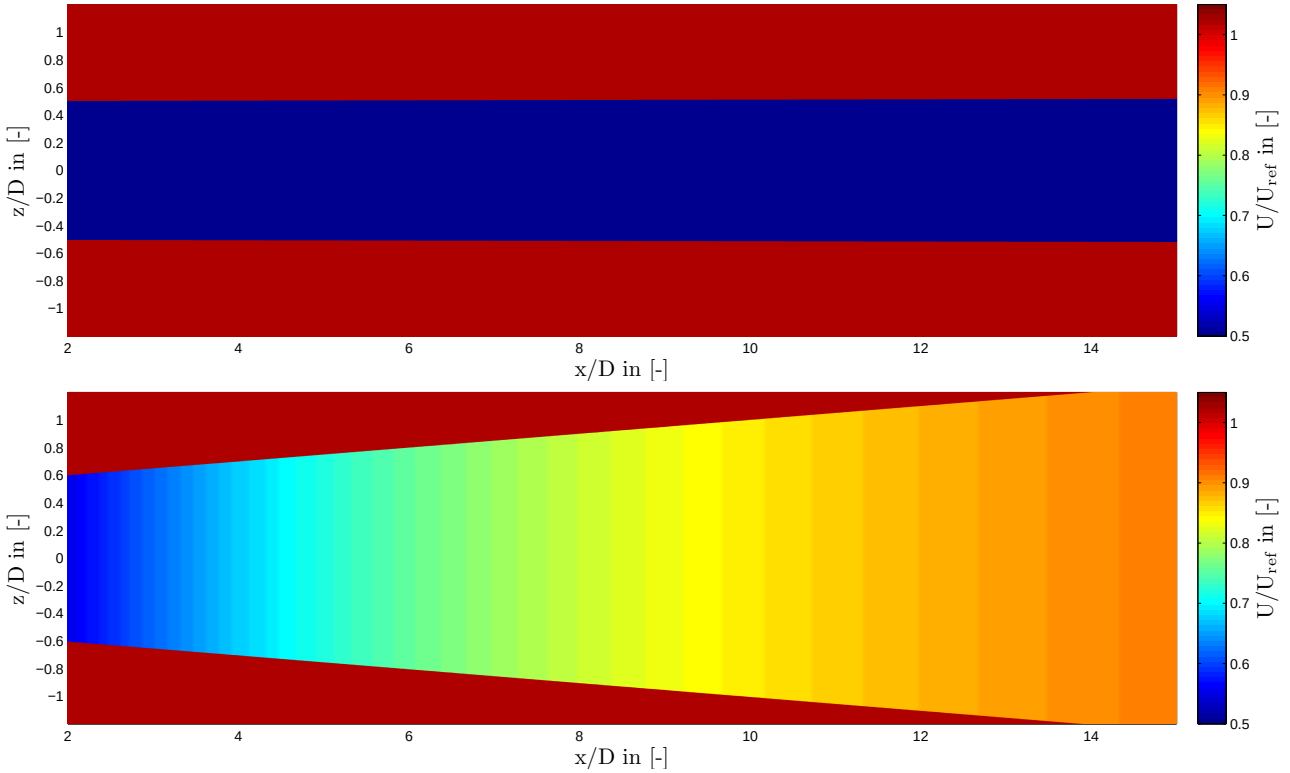

Figure B.3: Test case A: Jensen wake model results at hub height and **top:** $I_a = 0.23\,\%$, **bottom:** $I_a = 10\,\%$ at downstream distances $x/D = 2 - 15$

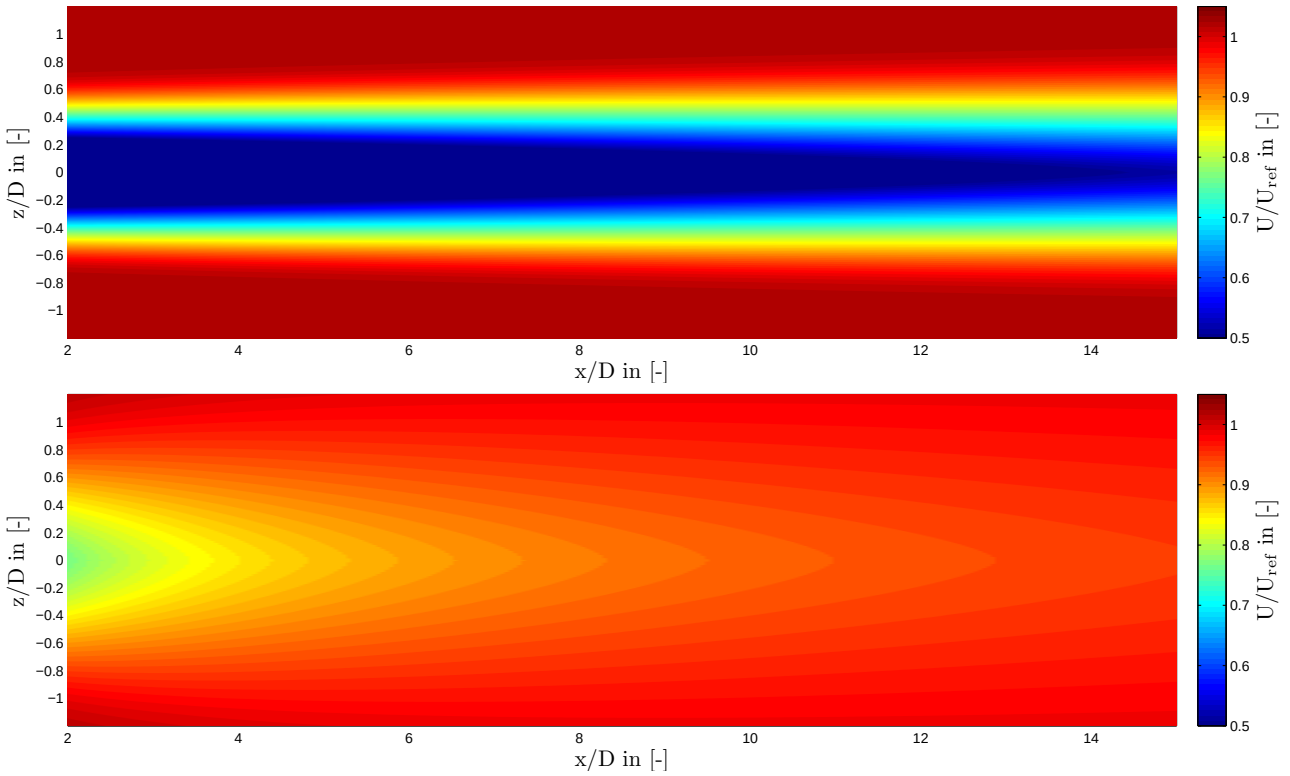

Figure B.4: Test case A: Larsen wake model results at hub height and **top:** $I_\mathrm{a} = 0.23\,\%$, **bottom:** $I_\mathrm{a} = 10\,\%$ at downstream distances $x/D = 2 - 15$

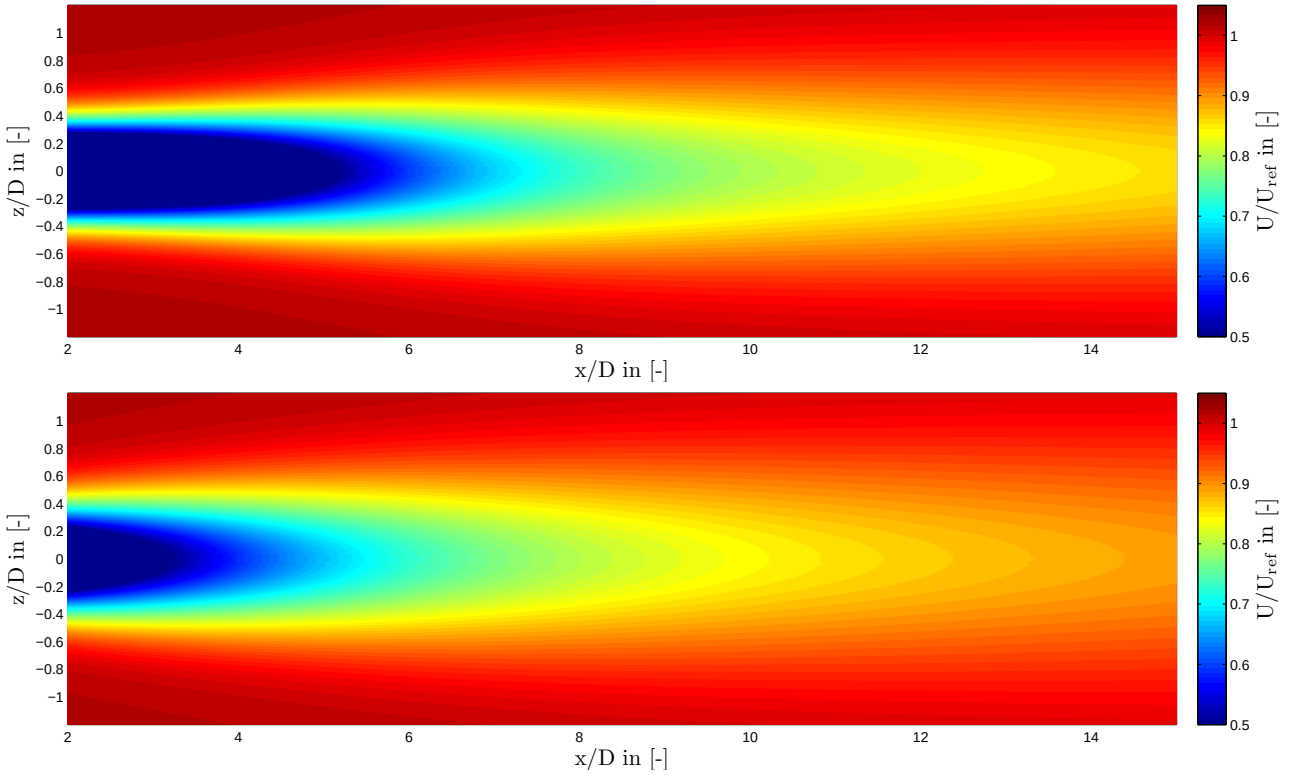

Figure B.5: Test case A: Ishihara wake model results at hub height and **top:** $I_\mathrm{a} = 0.23\,\%$, **bottom:** $I_\mathrm{a} = 10\,\%$ at downstream distances $x/D = 2 - 15$

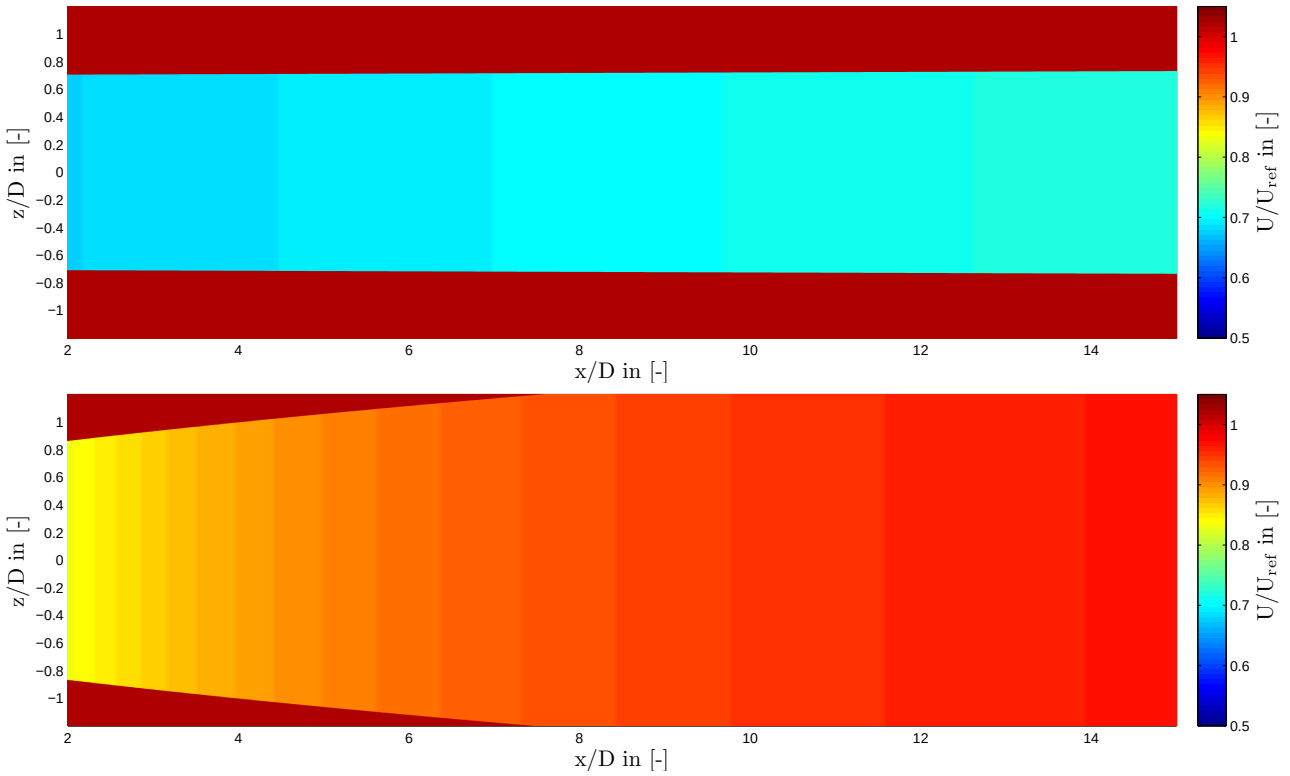

Figure B.6: Test case A: Frandsen wake model results at hub height and **top:** $I_a = 0.23\,\%$, **bottom:** $I_a = 10\,\%$ at downstream distances $x/D = 2 - 15$

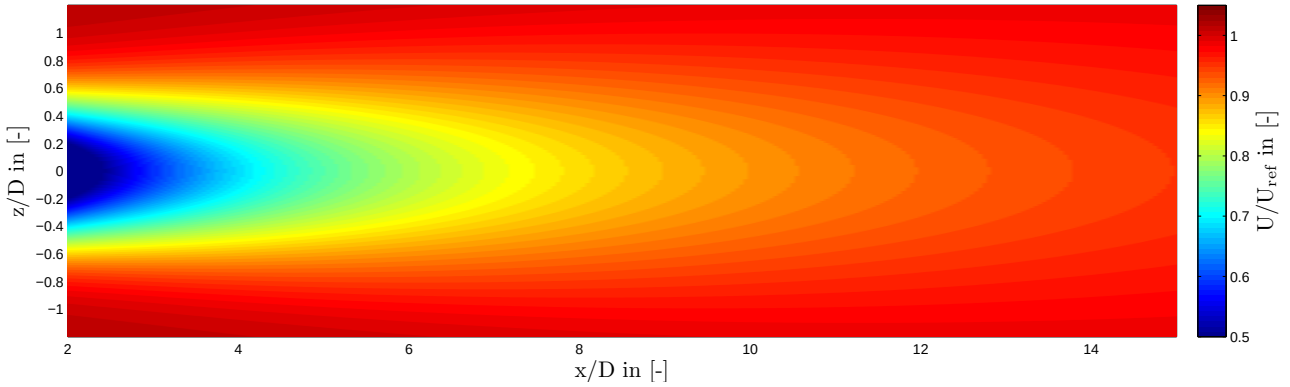

Figure B.7: Test case A: BP wake model results at hub height and $I_a = 10\,\%$ at downstream distances $x/D = 2 - 15$

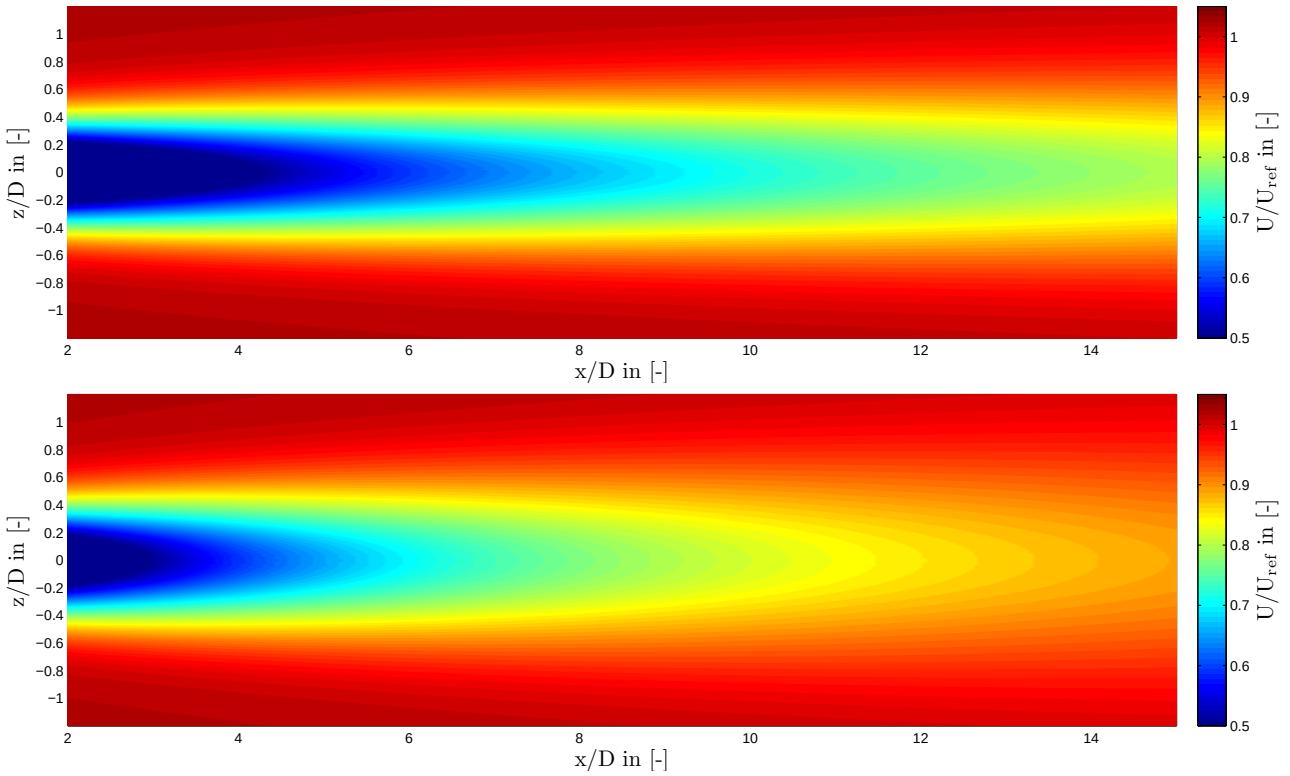

Figure B.8: Test case A: Jensen-Gaussian wake model plus Crespo and Hernandez turbulence model results at hub height and **top:** $I_a = 0.23\,\%$, **bottom:** $I_a = 10\,\%$ at downstream distances $x/D = 2 - 15$

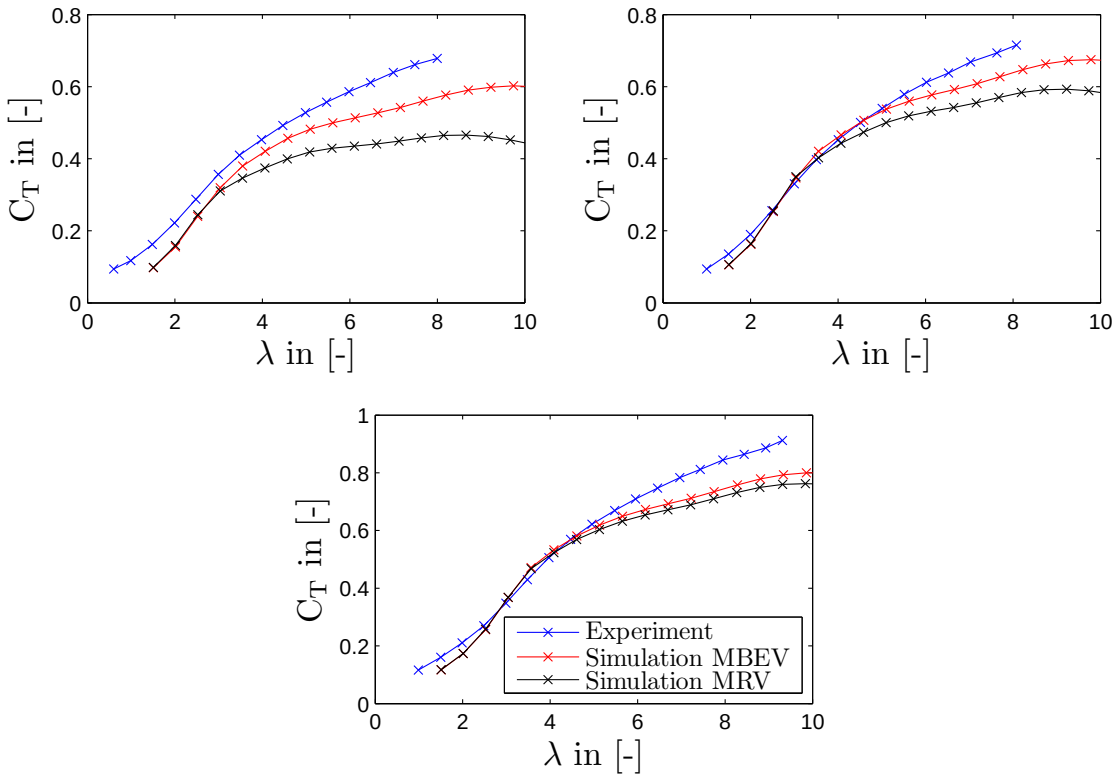

Figure B.9: Test Case C: Downstream turbine thrust measurement and modelling comparison using the mean-blade-element-velocity (MBEV) and mean-rotor-velocity (MRV) method at downstream distances **(top left:)** $x/D = 3$, **(top right:)** $x/D = 5$, **(bottom:)** $x/D = 9$ at upstream pitch angle $\beta = 0°$

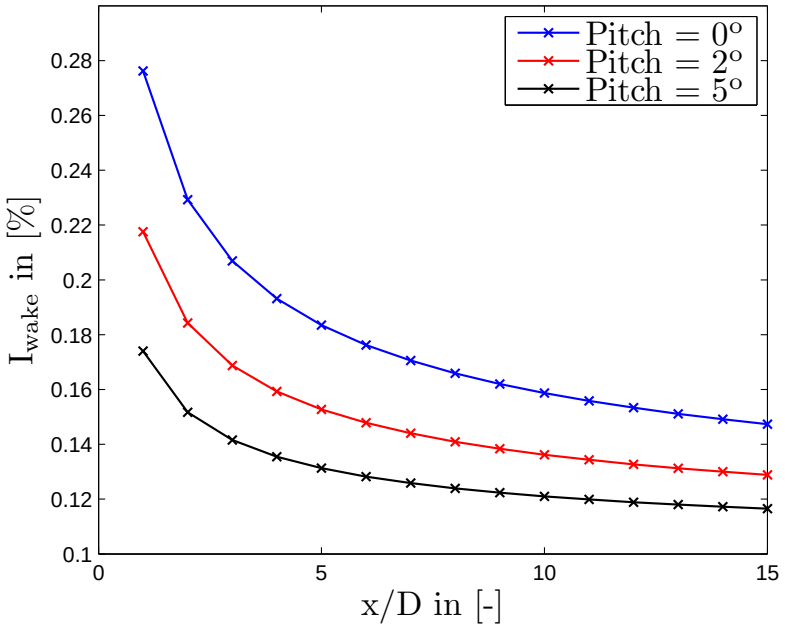

Figure B.10: Modelled wake turbulence intensity I_{wake} at upstream turbine blade pitch angles $\beta = 0°, \beta = 2°$ and 5° displayed at downstream distances $x/D = 1 - 15$ and ambient turbulence intensity $I_{\text{a}} = 10\,\%$ using the Crespo and Hernandez turbulence intensity model

C Appendix: Tables

Table C.1: Test case A: Wake prediction results using the comparison methods MAPE and APPE at both ambient turbulence intensities and downstream distances $x/D = 2 - 15$

		$I_a = 0.23\,\%$		$I_a = 10\,\%$	
		MAPE [%]	APPE [%]	MAPE [%]	APPE [%]
x/D = 2	Jensen	13.3	71.7	9.5	35.5
	Larsen	16.3	11.5	15.2	−105.7
	Frandsen	16.7	−104.8	17.4	−122.7
	Ishihara	22.8	49.0	14.2	37.8
	BP	-	-	10.1	30.8
	JGWM	17.5	−15.3	12.3	17.0
x/D = 3	Jensen	15.5	78.7	8.5	19.5
	Larsen	13.1	28.9	14.8	−106.9
	Frandsen	12.4	−52.5	16.4	−118.9
	Ishihara	16.9	45.8	7.2	15.7
	BP	-	-	5.1	−3.8
	JGWM	12.6	−7.8	6.9	4.5
x/D = 4	Jensen	17.4	82.1	7.4	10.3
	Larsen	10.0	36.7	13.5	−94.4
	Frandsen	8.1	−26.9	15.5	−104.3
	Ishihara	10.7	32.2	3.8	3.2
	BP	-	-	5.3	−19.2
	JGWM	8.0	−5.4	3.9	−0.5
x/D = 5	Jensen	17.3	80.8	7.4	4.9
	Larsen	8.0	28.5	12.1	−80.4
	Frandsen	8.4	−35.2	14.3	−89.2
	Ishihara	5.6	−3.8	2.5	−4.1
	BP	-	-	5.9	−25.6
	JGWM	5.8	−27.1	2.7	−2.2
x/D = 6	Jensen	18.6	83.4	7.1	2.7
	Larsen	7.9	35.7	10.4	−66.2
	Frandsen	6.7	−15.4	12.2	−74.3
	Ishihara	3.6	−16.8	2.6	−6.8
	BP	-	-	5.8	−26.5
	JGWM	3.9	−19.4	2.0	−1.6
x/D = 7	Jensen	19.3	84.2	7.6	0.5
	Larsen	7.7	36.6	9.3	−56.3
	Frandsen	6.1	−8.6	11.4	−64.0
	Ishihara	5.1	−33.3	3.0	−8.6
	BP	-	-	5.8	−27.0
	JGWM	3.8	−21.5	1.8	−1.7
x/D = 8	Jensen	20.0	85.5	7.2	3.7
	Larsen	8.1	39.9	7.8	−41.2
	Frandsen	5.5	1.3	9.7	−48.4
	Ishihara	5.6	−37.6	3.1	−3.8
	BP	-	-	5.4	−20.6
	JGWM	3.5	−17.8	2.5	3.0
x/D = 9	Jensen	20.8	86.9	6.9	3.2
	Larsen	8.7	44.2	6.9	−34.2
	Frandsen	5.6	11.7	8.8	−41.0
	Ishihara	5.4	−33.6	2.9	−2.6
	BP	-	-	5.1	−19.1
	JGWM	3.0	−11.1	2.6	3.7

		$I_a = 0.23\,\%$		$I_a = 10\,\%$	
		MAPE [%]	APPE [%]	MAPE [%]	APPE [%]
x/D = 10	Jensen	21.4	87.8	6.7	2.6
	Larsen	9.1	46.5	6.1	−28.8
	Frandsen	6.4	18.1	7.8	−35.5
	Ishihara	5.1	−30.7	2.8	−1.5
	BP	-	-	4.8	−17.9
	JGWM	2.7	−7.8	2.7	3.9
x/D = 11	Jensen	21.7	88.3	5.8	0.9
	Larsen	9.3	47.9	5.6	−26.0
	Frandsen	7.3	22.7	7.3	−32.6
	Ishihara	4.7	−27.9	2.7	−1.6
	BP	-	-	4.7	−18.3
	JGWM	2.6	−5.7	2.4	2.8
x/D = 12	Jensen	22.1	88.5	6.1	0.2
	Larsen	9.5	47.7	4.9	−22.7
	Frandsen	7.8	24.6	6.4	−29.2
	Ishihara	4.8	−27.9	2.4	−0.8
	BP	-	-	4.3	−17.6
	JGWM	2.5	−6.6	2.2	2.6
x/D = 13	Jensen	22.2	89.0	5.2	−1.9
	Larsen	9.6	49.0	4.7	−21.7
	Frandsen	8.5	28.4	6.1	−28.2
	Ishihara	4.2	−23.8	2.1	−1.5
	BP	-	-	4.3	−18.6
	JGWM	2.4	−4.2	1.8	1.0
x/D = 14	Jensen	22.5	89.3	5.5	−2.9
	Larsen	9.8	49.7	4.2	−20
	Frandsen	9.2	31.0	5.5	−26.3
	Ishihara	4.0	−21	1.9	−1.3
	BP	-	-	4.0	−18.5
	JGWM	2.1	−2.9	1.6	0.2
x/D = 15	Jensen	22.3	89.3	4.9	−5.0
	Larsen	9.6	49.2	4.1	−19.8
	Frandsen	9.4	31.8	5.3	−26.2
	Ishihara	3.7	−20.9	1.7	−2.3
	BP	-	-	4.0	−19.7
	JGWM	1.9	−3.8	1.5	−1.6